Cosmogenic nuclide production within the atmosphere and long period comets

BY

Andrew C. Overholt

Submitted to the graduate degree program in Physics and Astronomy

and the Graduate Faculty of the University of Kansas

in partial fulfillment of the requirements for the degree of Doctor of Philosophy.

_____

Chairperson Adrian Melott

_____

Bruce Lieberman

_____

Brian Thomas

_____

Bruce Twarog

_____

Graham Wilson

Date Defended: 3/7/2013

The Dissertation Committee for Andrew C. Overholt

certifies that this is the approved version of the following dissertation:

Cosmogenic nuclide production within the atmosphere and long period comets

_____

Chairperson Adrian Melott

Date approved: 3/9/2013

Abstract

The Earth is constantly bombarded by cosmic rays. These high energy particles collide with target nuclei, producing a shower of secondary particles. These secondaries contribute significantly to the radiation background at sea level and in the atmosphere, as well as producing rare cosmogenic nuclides. This contribution is variable over long time scales as astrophysical events change the cosmic ray flux incident on the Earth. Our work re-examines a previously proposed climate effect of increased cosmic ray flux due to galactic location. Although our work does not support this effect, cosmic ray secondaries remain a threat to terrestrial biota. We calculate the cosmogenic neutron flux within the atmosphere as a function of primary spectrum. This work is pivotal in determining the radiation dose due to any arbitrary astrophysical event where the primary spectrum is known. Additionally, this work can be used to determine the cosmogenic nuclide production from such an event. These neutrons are the fundamental source of cosmogenic nuclides within our atmosphere and extraterrestrial matter. We explore the idea that excursions in ^{14}C and ^{10}Be abundances in the atmosphere may arise from direct deposition by long-period comet impacts, and those in ^{26}Al from any bolide. We find that the amount of nuclide mass on large long-period comets entering the Earth's atmosphere may be sufficient for creating anomalies in the records of ^{14}C and ^{10}Be from past impacts. In particular, the estimated mass of the proposed Younger Dryas comet is consistent with its having deposited sufficient isotopes to account for recorded nuclide increases at that time. The $^{26}Al/^{10}Be$ ratio is much larger in extraterrestrial objects than in the atmosphere,

and so, we note that measuring this ratio in ice cores is a suitable further test for the Younger Dryas impact hypothesis. This portion of our work may be used to find possible impact events in the geologic record as well as determination of a large bolide impact rate.

Acknowledgments

First and foremost I would like to thank God. Everything good in my life can be traced back to Him and His influence on me and everyone around me. I only hope that I am using the blessings He has poured out on me in the way He would have me. Without His strength, His guidance, and His unfailing love, I wouldn't make it out of bed in the morning, much less have the strength to do physics.

When I took General Physics I as a freshmen at Southern Nazarene University, I had no idea what path that act would set me on. Though there have been high points and low points during the years which I have pursued my doctorate, the wonderful people who have helped me along the way made it possible.

During my undergraduate career I had the amazing privilege of taking my physics classes from Dr. Dwight E. Neuenschwander. With an infectious passion for physics and a challenging curriculum, he prepared me for graduate school like I do not believe anyone else could. Without his support and patience I am unsure if I would have pursued physics to the degree which I have.

I would also like to thank the graduate faculty of the University of Kansas. My classes at KU prepared me for research and gave me a base from which to explore the depths of my field. These classes showed me how deep and rich the subject of physics really is, a point of view I hope to share with my students. Thanks must also be given to my committee, who gave me great feedback through my entire doctoral process and helped direct me towards important areas where I needed improvement. I wish everyone

pursuing a doctorate could have a committee as knowledgeable, interested, and helpful as mine.

Special thanks goes to my research group, including Dr. Dimitra Atri and my advisor Dr. Adrian Melott. Dimitra performed CORSIKA calculations used in conjunction with this work which made this work possible. I cannot thank him enough for his contribution and guidance. Even more important is the contribution of my advisor. Dr. Melott has been an amazing advisor, giving me guidance, instruction, and a share of his wealth of knowledge on the subjects covered as part of this work. He pushed me when I needed pushing, and supported me when I needed supporting. There is no doubt that this is only possible because of his overwhelming support and contributions. I am excited to continue my work with him as a colleague and a friend.

Finally, I would like to thank my friends and family. I am not always the easiest person to stand behind, especially when I am stressed and frustrated about my code (or my writing, or any number of other research complications). My parents, Ed and Bettie Lou, raised me to work and to appreciate education. They have always loved me and shown an interest as well as pride in my work, and I can't thank them enough for that. My sister Corrie and brother David have always been there for me, supporting me even in times when they didn't know I needed it. My amazing friends and my church continue to support me every day and love me despite all of my vast shortcomings. Above all of them I would like to thank my wife, Jo. She put up with me when I know nobody else would. She continues to give me the strength to do things I never thought possible. I can't thank her enough for her life changing love. Jo, I love you.

Table of Contents

List of Figures

1. Introduction

Cosmic rays are particles primarily originating outside the solar system which are accelerated to high energies before colliding with the Earth's atmosphere or extraterrestrial matter. These particles are primarily protons with a small component of helium nuclei, heavier nuclei, and electrons. They interact with matter present in the atmosphere of planets as well as extraterrestrial matter such as comets. These interactions produce additional free particles, forming a cascade of secondary particles, those of which with sufficiently high energy interact to form additional secondaries. When these cascades occur within the Earth's atmosphere they are known as cosmic ray air showers. Although the effect of primaries is very small, the large number of secondaries makes them a significant source of additional interactions. The effects of cosmic ray secondaries are a significant area of research. Effects include ionization of the atmosphere, radiation from muons and neutrons, cosmogenic nuclide production from neutrons, as well as a proposed change in the Earth's climate (Shaviv 2003, Svensmark 2006, Svensmark et al. 2009).

Ionization of the Earth's atmosphere primarily occurs when the charged portion of cosmic ray showers interact with atmospheric matter. This charged portion contains muons, as well as less penetrating particles referred to as the soft component. This soft component includes protons, electrons, charged pions, and other charged particles formed in air showers. These particles do not penetrate deeply into our atmosphere due to their larger interaction cross section. For this reason we will not focus on the soft portion of

cosmic ray showers as they do not contribute to the radiation background nor create isotope variance through nuclear reaction.

The hard portion of cosmic ray showers contains muons and neutrons. These particles have a much smaller interaction cross section which allows them to penetrate deep into the atmosphere to ground level or below. With low energy (<1 GeV) cosmic rays, muons are not produced and neutrons do not penetrate the stratosphere. In the case of air showers produced by high energy cosmic rays, these particles are increased at ground level and below. These ground level particles become a source of radiation for terrestrial biota. Current rates of high energy cosmic rays make them an insignificant portion of the radiation background. However, these rates could increase to hazardous levels due to events such as supernovae, supernovae remnants, and the extragalactic shock model (Medvedev & Melott 2007). The amounts of increased radiation from such events are unknown; however we have performed simulations of cosmic ray showers to approximate these increases. Our work, being independent of primary spectrum, is the first of its kind and as such is a necessary tool for exploring the effects of these events.

Due to magnetic confinement, there is an increased cosmic ray flux within the spiral arms of the galaxy (Shaviv 2003). This contribution is likely small, increasing cosmic ray flux on the Earth during spiral arm transit ~10-20%. Although this increased flux is too small to produce a measurable increase of ground level radiation, it has been proposed as the source of climate change on the Earth's surface through cloud nucleation (Shaviv 2003, Svensmark 2006). This effect is controversial (e.g. Erlykin et al. 2009,

Overholt et al. 2009, among others), and was tested against appropriate spiral arm locations as part of this work.

The hard component, primarily neutrons, is also known to create cosmogenic nuclides within target matter. These nuclides are rare and concentrations are measurable in some cases. Measurements of these rare cosmogenic nuclides have been used to determine the historic cosmic ray flux, however may also be used as a proxy for past impact events. As bolides such as meteors and comets spend their lifetime outside the protection of the Earth's magnetic field, they experience a greatly increased cosmic ray flux. Long-period comets spend the large majority of their lifetime outside of the heliosphere, where cosmic ray flux is larger still. This increased cosmic ray flux is known to create an abundance of cosmogenic nuclides which may be large enough for measurement in the geologic record in some cases. We explore this possibility as part of this work and apply our results to a controversial hypothetical impact event.

2. Sources of Cosmic Rays

2.1 Low Energy Cosmic Rays

Solar cosmic rays with energy from 10 to 100 MeV interact in the atmosphere (Ziegler 1996). Air showers of secondaries created in these collisions cause atmospheric effects, with very few of these particles reaching ground level (Melott et al. 2008, Vanio et al. 2009).

Among the most dangerous particles to biological systems and most likely to cause nuclear interactions are the neutrons and muons of the hard component (Vanio et al 2009). Neutrons are capable of initiating nuclear reactions, while muons also break chemical bonds. With low energy solar cosmic rays, neutrons are deposited in the stratosphere and pose a threat only to flight crews. Muons require a primary energy of ~1 GeV for production (Atri & Melott 2011a), eliminating solar cosmic rays as a primary producer of cosmogenic muons.

Low energy cosmic rays produce neutrons capable of cosmogenic nuclide production despite their lack of penetration. The most common isotope formed through solar cosmic rays is ^{14}C, though other examples such as ^{10}Be and ^{36}Cl exist. Though low energy cosmic rays produce fewer neutrons per primary, this energy range is the primary source of ^{14}C within our atmosphere, due to the large abundance of solar cosmic rays.

2.2 High Energy Cosmic Rays

Although most cosmic rays incident upon the Earth are solar in origin, higher energy cosmic rays (HECRs) from galactic sources will produce much stronger terrestrial effects when increased episodically. Galactic sources create cosmic rays from 100 MeV up to TeV and much higher ranges (Dermer & Holmes 2005, Smida 2009, Reitz 1993, Ackermann et al. 2013). There are many possible sources including supernovae, supernova remnants, and the bow shock of the Milky Way. They create a complex cosmic ray spectrum with two separate breaks, one at ~10^{15} eV, and one at ~10^{18} eV (Ptuskin 2005, Raymond 2009, among others). It has been shown that young supernovae accelerate particles up to 100 TeV (Vink 2009, Ackermann et al. 2013). Though there has been extensive investigation of effects from X-ray and gamma-ray photons on Earth (Ruderman 1974, Scalo & Wheeler 2002, Karam 2002b, Gehrels et al. 2003, Melott et al. 2004, Thomas et al. 2005a, Melott et al. 2005, Thomas et al. 2005b, Thomas et al. 2006, Ejzak et al. 2007, Thomas et al. 2008, Melott & Thomas 2009) less has been made at computing HECR effects (Gehrels et al. 2003, Melott et al. 2008, Atri & Melott 2011a, Atri & Melott 2011b).

HECRs penetrate further into the atmosphere and create a large flux of particles at the surface of the Earth. This is due to the increased energy of the primary causing increased momentum in the secondaries dispersing them farther below the initial interaction. Their penetration makes them a greater a threat to terrestrial life than solar cosmic rays.

2.3 Time Variability of Cosmic Ray Flux

Though the cosmic ray spectrum is constant on the Earth on short time scales, there are a variety of phenomena which increase the cosmic ray flux on the Earth episodically over long time scales. These astrophysical events include solar proton events (SPEs) originating in the Sun, supernova remnants, and possibly the bow shock of the galaxy as it moves through space (Medvedev & Melott 2007). As there are many different phenomena which increase cosmic ray flux on the Earth, these events vary significantly in duration, frequency, and magnitude.

Cosmic ray flux increasing events vary in duration from less than one year to millions of years. SPEs generate cosmic rays suddenly as protons emitted by the Sun become accelerated to high energies during a solar flare or by the shocks associated with coronal mass ejections (CMEs). These events are very short lived in comparison to other astrophysical phenomena, often lasting less than 48 hours. The cosmic rays of supernovae diffuse through interstellar space due to magnetic turbulence. This diffusion is often approximated by a statistical random walk, increasing the residence time of cosmic rays in the Galaxy substantially. Though a supernova is a short lived event, the increased cosmic ray flux on the Earth from such an event would last ~1 kyr due to cosmic ray diffusion. The galactic bow shock is a potential source of high energy cosmic rays. These cosmic rays are accelerated along the magnetic field lines of the shock

through Fermi acceleration (Medvedev & Melott 2007). Although this phenomenon creates a continual increase in cosmic ray flux, the Earth would only be exposed to this flux every ~60 Myr. This exposure occurs as the sun moves outside of the protection of the galactic plane. Thus, the duration of the cosmic ray flux increase on Earth is thought to be millions of years, the same as the Sun's residence time outside of the galactic plane.

The frequency of cosmic ray flux increasing events is highly variable, similar to event duration. The frequency of intermittent intense ionizing radiation sources has been estimated (Melott & Thomas 2011); however this does not include all HECR flux increasing events. Solar events are much more frequent than other astrophysical sources, with many small events occurring annually. The frequency of supernova produced cosmic ray exposure is dependent on stellar density and supernova rate. These events are thought to be much rarer, with significant events only becoming probable on long time scales (Melott & Thomas 2011). The galactic bow shock increases the Earth's exposure to cosmic rays periodically. The Sun's motion exposes it to increased cosmic rays from the galactic bow shock every ~60 Myr according to this model (Medvedev & Melott 2011). Although these two phenomena are much more infrequent than solar events, they are of much greater magnitude.

The terrestrial cosmic ray flux increases episodically as the Earth is exposed to cosmic ray producing events. The amount of increase experienced depends upon the total energy of the astrophysical event. Whereas solar events only produce small adjustments to the cosmic ray flux on the Earth, other astrophysical events are capable of producing very large increases in HECR flux. Nearby supernovae produce the largest HECR flux

increase. These events are capable of producing flux increases which threaten terrestrial life through secondary particle radiation. Although such events are decidedly rare, they remain statistically probable on timescales encompassed by the geologic record.

2.4 Spiral Arm Transit

The spiral arms of our galaxy are regions of high stellar density within the pattern of our galaxy. These regions of space contain an increased cosmic ray density due to the confinement of charged ions by the magnetic fields of stars within the region. Magnetic trapping will affect both low and high energy cosmic rays. Although low energy cosmic ray flux is increased in these regions of trapping, the Earth is mostly shielded from these particles by the heliosphere. For this reason the terrestrial effects are dominated by high energy cosmic rays which pass the heliosphere. Our location relative to these regions changes as the sun orbits the galactic center. This has led to some speculation regarding the possible effects of transit in and out of the high stellar density spiral arms. We will now examine more closely one of the effects suggested: climate temperature decreases caused by increased cosmic ray flux.

2.4.1 Climate Correlation

In recent years there have been suggestions of a strong correlation between spiral-arm passages of the Sun in its orbit around the Galaxy and changes in the terrestrial climate. This connection has been based on a statistical association of spiral-arm passages with the timing of ice ages as well as the abundance of ^{18}O in fossils, which is linked to the ocean water isotopic ratio. The ^{18}O in the ocean is enriched when ^{16}O water preferentially evaporates and is retained within ice. The presumed mechanism for the climate change is thought to be an increase in cosmic rays that may affect cloud formation.

As the solar system passes through the spiral arms of our galaxy, it is exposed to an increased rate of cosmic rays from more frequent regional supernovae and stronger cosmic-ray confinement on account of a higher amplitude of magnetic turbulence. One model suggests that cosmic ray secondary particles may be responsible for an increased number of low clouds being formed, thus blocking sunlight and cooling the climate (Svensmark 2006). Previous work on this subject has suggested that these spiral-arm crossings and the resultant increase in cosmic rays would therefore decrease the overall temperature of the planet (Shaviv 2003, Shaviv & Veizer 2003). This suggested mechanism is controversial, both on grounds of the weak response of cloud-condensation nuclei to changes in the cosmic-ray flux (e.g. Pierce & Adams 2009), and on geological

grounds (Rahmstorf et. al. 2004), but the controversy continues: see Erlykin et al. (2009), Svensmark et al. (2009), and Overholt et al. (2009). We do not address this mechanism here, or conflicting geological arguments, but rather investigate whether the correlation between spiral-arm passage and climate holds up under newer information on the structure of the Galaxy.

Since the primary publications on the spiral-arm passage and climate correlation, newer models of the galactic structure, including the positions of the spiral arms, have been created that place our transit of these spiral arms at a different time. Models of the galactic structure have been formulated to overcome the difficulties of observing the Galaxy from our position within the disk, using as tracers H II regions, open star clusters, FIR dust loops, or velocimetric deconvolution of CO and H I data (for a review see Vallée 2008). These made a fit to the data assuming 2, 4, or more symmetric, logarithmic spiral arms (e.g., Wainscoat 1992, Goncharov & Orlov 2003, Russeil 2003, Minchev & Quillan 2008, Gillman & Erenler 2008, Vallée 2008, etc.). Of course the resulting spiral-arm models feature symmetric spiral arms, because only those were allowed. This is neither proof nor evidence for the arms actually being symmetric. The velocimetric deconvolution of CO and H I has its own difficulties (Gomez 2006) and is conventionally performed assuming a purely circular flow of matter around the Galactic Center (e.g. Nakanishi & Sofue 2006). More complex flows are known to exist in the spiral arms themselves (e.g. Russeil et al. 2007), but also throughout the inner Galaxy, where the galactic bar induces a strong azimuthal asymmetry in the gravitational potential (Bissantz et al. 2003). Though nearly all current models of the Milky Way have four spiral arms,

the method of fitting them varies widely. Most models force spiral arms into particular fits such as logarithmic arcs originating in the center of the galaxy (Vallée 2008). The model we will be using does not force-fit any presupposed pattern but rather is based on density enhancements of CO gas (Englmaier et al. 2008). This fixes more accurately and completely the position of the spiral arms especially on the far side of the Milky Way. We present results of a re-examination of the previously found correlation between spiral arm crossings and the climate of Earth in light of new information on the Milky Way. It will be shown that due to the asymmetric position of the spiral arms, the correlation dissolves in this newer model and no periodic trend due to the passage of arms on less than the total orbital period is possible.

2.4.1.1 Galactic Structure

We will now examine the spiral-arm crossing locations in the more recent and complete view of the current galactic model. The models chosen take into consideration new criteria for spiral arms that do not force-fit them to logarithmic arcs (Englmaier et al. 2008). These models are based on the density of CO gas, which was recently modeled using a gas-flow model derived from smoothed particle hydrodynamics (SPH) simulations in gravitational potentials based on the NIR luminosity distribution of the bulge and disk (Bissantz et al. 2003). Besides providing a more accurate picture of cloud orbits in the inner Galaxy, a fundamental advantage of this model is that it provides

kinematic resolution toward the Galactic center (Pohl et al. 2008), in contrast to standard deconvolution techniques based on purely circular rotation. To estimate the magnitude of systematic errors in the deconvolution, three different gas-flow models for the inner Galaxy were investigated, one of which was intentionally distorted so it no longer corresponds to a SPH simulation that has been adapted to gas data. A mismatch of the gas-flow model led to a significant increase in the number of artifacts, this allowed a quality ranking of models (for different bar parameters, etc.). In the inner Galaxy, where the CO line signal is strong enough and molecular clouds are presumed to trace the spiral arms due to their large density, Pohl et al. (2008) note that two spiral arms seem to emerge at the ends of the bar, which have a small pitch angle. While some structures in the surface density distribution may be associated with two more arms, the evidence for those arms is not strong in their deconvolution. Englmaier et al. (2008) have compiled a composite model of the gas distribution in the Milky Way, using the CO distribution model for the inner Galaxy (galactocentric radii less than 8 kpc) where the SPH gas-flow model is available and CO line intensities are high, and a H I deconvolution from the literature (Levine et al. 2006) for the outer Galaxy, where the H I line provides a stronger signal and the asymmetry introduced by the galactic bar is small.

The resulting model of our Galaxy is shown in Fig 1. Since the spiral arms are matched to structure seen in the deprojected gas-distribution map, there is no reason to expect symmetry in the derived spiral pattern. However, one nevertheless finds an almost perfect 180-degree rotational symmetry in the inner Galaxy. At the solar circle the CO and H I deconvolutions match very well, thus reinforcing a sensible connection between

the spiral arms in the inner and outer Galaxy. Spiral arms cannot cross, only branch (Englmaier et al. 2008). The 2-armed spiral pattern in the inner Galaxy, branches in two more arms at about the solar circle, resulting in an asymmetric location of spiral arms. Such asymmetry cannot be captured in the published studies (Vallée 2008), because they fit symmetric spiral-arm models. This gives us a better location for the Scutum-Crux arm, which is important for this work.

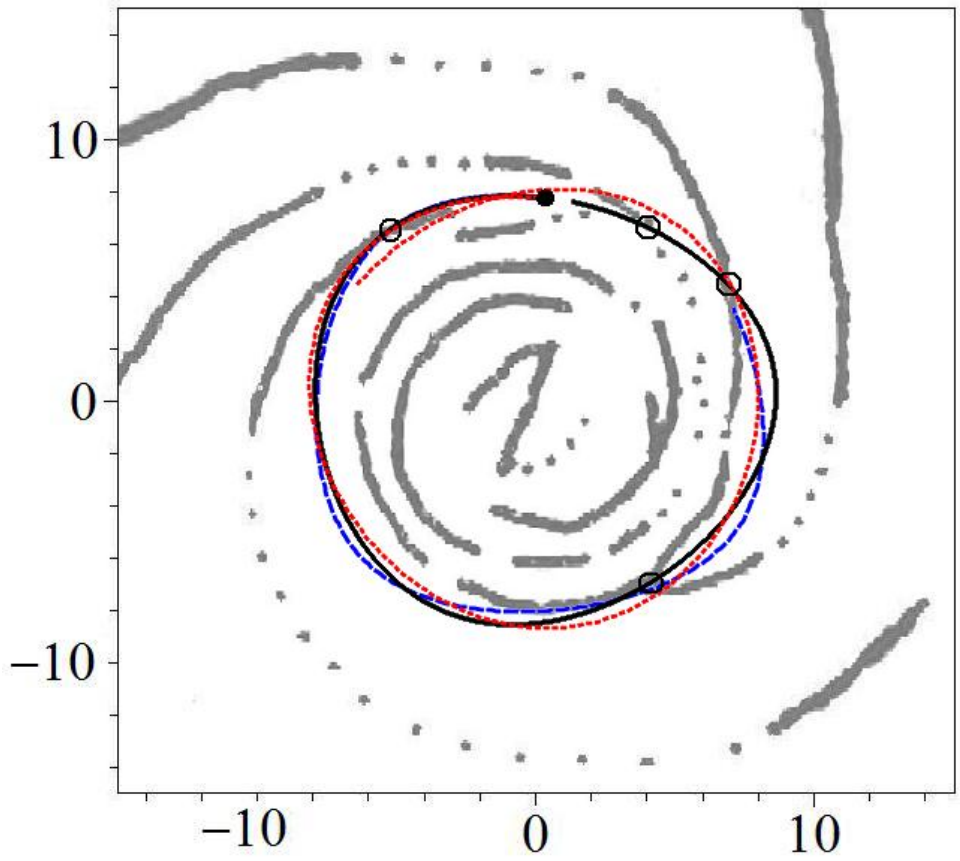

Figure 1: The path of our Solar System through the spiral arms of the Milky Way, as defined by high-density molecular-cloud data (Englmaier et al. 2008). The heavy black line is the trajectory of our Solar System relative to the galactic pattern when the difference in speeds is 11.9 km s^{-1} kpc^{-1}. The blue dashed line represents the lower bound of the previously assumed pattern speed difference, 10.1 km s^{-1} kpc^{-1}; while the red dotted line represents the upper bound of the previously assumed pattern speed difference, 13.7 km s^{-1} kpc^{-1} (Shaviv 2003, Gies & Helsel 2005, Svensmark 2006). Our current location in the Galaxy is shown as a black dot, and the empty circles represent the intersections with the spiral arms. Axes are labeled in kpc. From Overholt et al. (2009).

Although the speed of our solar system in its orbit around the Galactic Center is known to sufficient precision, the density-wave propagation speed of the spiral pattern is not. This pattern speed would have a dramatic effect on the intersection times we are modeling. Previous work on this subject has allowed the pattern speed to vary, and some studies suggest the co-rotation radius is close to the solar circle, meaning the spiral-arm pattern speed and the orbital angular velocity of our solar system may be very similar (e.g., Marochnik et al. 1972, Dias & Lépine 2005, etc.), in which case the period of spiral-arm passages would be much longer than the timescales of terrestrial climate change, 140 Myr. Gies & Helsel (2005) found extremely good fit to terrestrial variables for a difference between pattern speed and the orbital angular velocity of the solar system of 11.9 km s^{-1} kpc^{-1}. They also considered a speed difference of 6.3 km s^{-1} kpc^{-1}, but that does not agree as closely with the terrestrial variables, regardless of galactic model. Other work on the subject puts the difference in speeds at the value of 12.3 km s^{-1} kpc^{-1} (Svensmark 2006), and 11.1 km s^{-1} kpc^{-1} (Shaviv 2003). It appears that any speed difference between 1 and 13.5 km s^{-1} kpc^{-1} could be considered plausible (Shaviv 2003). Variations in the star-formation history of the Milky Way do not provide useful constraints on the spiral-arm pattern speed, because the time resolution is not high enough and because of orbit diffusion on Gyr-timescales (Rocha-Pinto et al. 2000).

The solar trajectory found by Gies & Helsel (2005) uses cylindrical coordinates and bases the current position of the solar system on the model (model 2) developed by Dehnen & Binney (1998). This model places our sun starting at a distance of R_0=8.0 kpc and gives the solar system a circular velocity at that location of 217.4 km s-1. From these

starting parameters the trajectory was then numerically integrated backwards in time 500 Myr with time steps of 0.01 Myr to develop the elliptical orbit of our sun about the Galactic Center. As this path is elliptical, the solar motion relative to the galactic pattern will not be circular, but rather will vary in radius with a period less than the orbital period. Motion in the Z direction (normal to the galactic plane) is ignored as this will only slightly modify the intersection times and not change the pattern of intersections. The motion relative to the pattern is found by subtracting off the motion due to the assumed pattern speed. This assumes a constant pattern speed throughout the region defined by the variance in radius of the solar trajectory. Although this is assumed, velocity fields in this region based on the gas flow model of Bissantz et al. (2003) finds the velocity distortions to be less than 10 km s^{-1}, much less than the ~200 km s^{-1} orbit velocity at the solar radius. Including the systematic errors in the gravitational potential, we estimate the error in the calculated solar trajectory to be below 10% and thus negligible in comparison with the uncertainty of the spiral-arm pattern speed. We also posit that all spiral arms have a common pattern speed. Freely assigning independent pattern speeds to the spiral arms introduces four free parameters (being the independent arm speeds), and in the light of only seven climate events to be reproduced simply violates Occam's razor. Intersections were then found as angles where the solar orbit and spiral arms coincide. These angles of intersection then correspond to the times given in Fig 2. Plotted against these points of intersection are vertical lines indicating the time of the last seven "Ice Age Epochs" (IAEs; Shaviv 2003). It should be noted at this time that the intersections are now quite asymmetric, mirroring the asymmetry present in our

galactic picture. Whereas in previous work only periodic consequences of these crossings were considered, this new picture of the galaxy shows a lack of periodicity due to the asymmetry.

2.4.1.2 Key Connections to Terrestrial Climate

Many different correlations between galactic position and the Earth's climate have been found, we will now re-examine those correlations in the light of the new galactic picture. For a record of Earth's climate we will both be using $\delta^{18}O$, as well as the times of the assumed IAEs over the last 1 Gyr. Two crucial linchpins of this work are a 140-Myr cycle apparent in both the oxygen data and the IAEs (Shaviv 2003, Shaviv & Veizer 2003). This strong 140-Myr cycle describes a massive temperature change unexplained as of yet by terrestrial causes. A similar and unexplained periodicity is also seen in biodiversity studies (Melott 2008, Melott & Bambach 2009), but is not statistically robust at this time. The other important connection is the implied relatively recent transit of the Scutum-Crux spiral arm, linked to a probable cold period in the mid to late Jurassic (Shaviv 2003, Svensmark 2006).

We examine the path of the Sun relative to the spiral structure evident in Figure 1. The results are very different from those seen before. Though the solar motion now includes the elliptical path found by Gies & Helsel (2005), the motion is still very close

to circular. The differences thus lie in the location of the spiral-arms in the new model and the new intersection angles.

2.4.1.3 Results

As the new galactic structure is not symmetric, having dropped the former force-fit symmetry assumptions, it is impossible to produce a 140-Myr periodic spiral arm passage time. Figure 2 shows the timing of ice ages, the times of spiral arm passages found before, and those found with the new structural information. Horizontal error bars represent the time that the Sun's orbital path skims along inside or very close to one spiral arm. The only periodic trend that can be found with the new data is the relative orbital period of our solar system (Gies & Helsel 2005) relative to the previously assumed pattern speed around the galactic plane, which is slightly larger than 500 Myr. Though one could create varying periodic trends by changing this pattern speed, the orbital period relative to the galactic pattern could never reach the 140 Myr time as this is less than the orbital period itself, meaning the pattern and the Sun would be required to move in opposite directions.

We have checked the effect of varying the pattern speed in light of the elliptical orbit, and this does not introduce any improved fit to the geological data. Speeds were sampled at increments of 0.001 km s-1 kpc-1, the resulting hits are found in Figure 3. Both the range used and the optimal speed that was chosen agreed with previous work

(Shaviv 2003, Gies & Helsel 2005, Svensmark 2006). In this case, the optimal speed difference is 11.9 km s^{-1} kpc^{-1}. Secondly, the Scutum-Crux spiral arm passage, key to fitting some of the most recent and reliable geological data, simply does not happen. The Sun never passes closer than 2 kpc to this spiral arm.

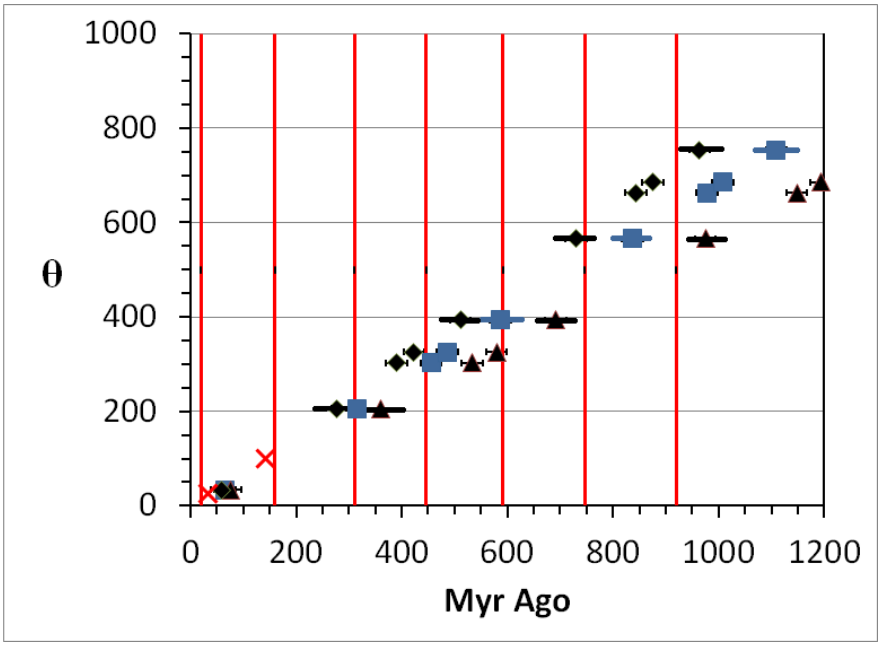

Figure 2: Red vertical lines represent the midpoints of the last seven ice ages (Shaviv 2003) showing the reported 140-Myr climatic cycle, red X's marking the intersections of the Solar System with spiral arms found in previous work (Svensmark 2006). They assumed the spiral arm crossings to extend in a 140-Myr periodic pattern. Intersections of our Solar System with the spiral arms of the Milky Way computed from the current model are plotted in blue squares, with upper bounds of pattern speed plotted in black triangles and lower bounds of pattern speed giving the intersections plotted in black diamonds, showing lack of correlation to the ice age epochs within the given pattern speed range. Error bars on intersection points represent combined error of ice age epoch time and spiral arm intersection uncertainty of 20 Myr. Horizontal bars represent the extended intersection time for grazing events. Angles are taken in degrees from current location, increasing with time into the past. From Overholt et al. (2009).

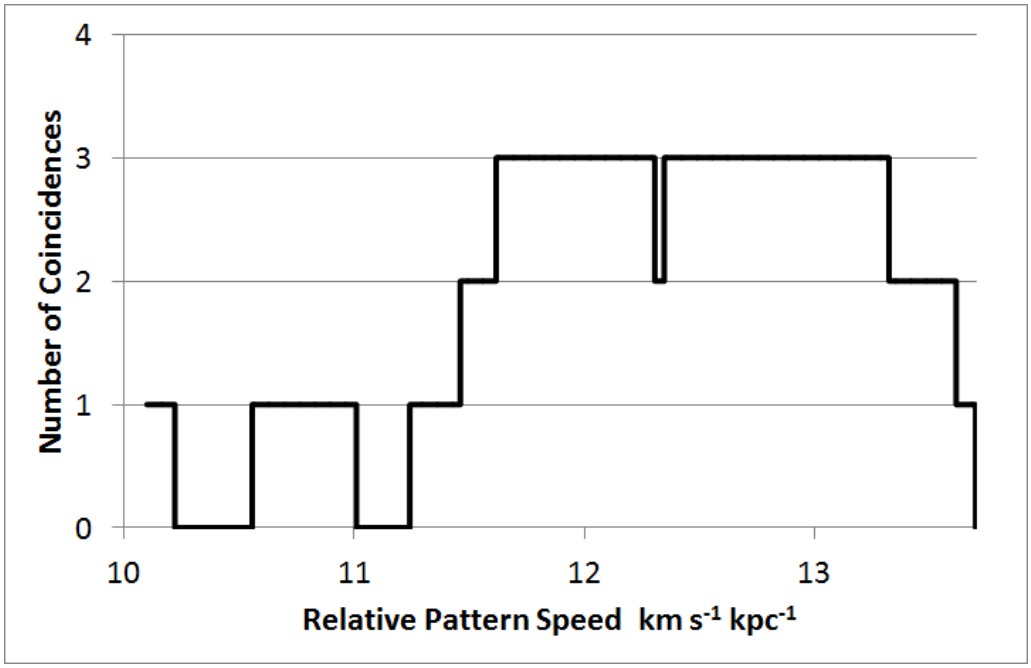

Figure 3: The number of coincidences between spiral arm intersection and ice age epochs are plotted in black. Results are plotted relative to pattern speed difference in increments of 0.001 km s^{-1} kpc^{-1}, ranging from 10.1 to 13.7 km s^{-1} kpc^{-1}, after Svensmark (2006) and Shaviv (2003). Included in the calculation is the 15.4 Myr cosmic ray lag (Shaviv 2003), however similar results with no greater hits are produced if this lag is omitted.

It is important to note that since the spiral structure is not symmetric, a strict periodicity in the intersection of the solar orbit with spiral arms is not indicated. But the more fundamental question is whether there is evidence supporting the association of spiral-arm crossings with terrestrial glacial episodes. Figure 2 shows eight spiral arm crossings and seven glacial periods in the time considered (up to 1000 Myr ago). These calculations incorporate a 15.4 Myr lag due to cosmic ray diffusion after Shaviv (2003). Without this effect, the number of agreements between ice age epochs and spiral arm crossings is unchanged. We can roughly estimate the significance of the association that emerged. Given error bars on the glacial timings of ± 10 to 20 Myr, and variable but similar duration of the spiral arm crossing timings, we allow up to 20 Myr difference in timing to be recorded as an agreement. With this choice, we count three coincidences from eight opportunities (eight spiral arm crossings which might coincide with a glacial period). There are therefore five spiral arm crossings which do not have coincident glacial periods. Allowing ± 20 Myr between the timing of the two events still being counted as agreement means that 0.286 fraction of each ~140 Myr period would be counted as agreement. The binomial probability of having three or more hits out of eight trials with this probability is 0.413. Thus there is a ~41% chance that the association seen in Figure 2 is simply the result of random placement. This does not take into account the fact that this plot was manufactured based on the optimum pattern speed assumption—the one which produced the greatest number of hits. Alternative pattern speeds within the given range all produce fewer hits.

We therefore cannot reject the null hypothesis that there is there is no correlation between spiral arm crossings and ice age epochs, even by optimizing the pattern speed. Our findings therefore do not support a correlation between spiral arm crossings and ice ages.

2.4.1.4 Discussion

Although previous work found a correlation between the 140-Myr climate cycle on Earth and the intersection with spiral arms (Shaviv 2003, Shaviv & Veizer 2003, Svensmark 2006), with new data on the structure of the Galaxy, this correlation disappears. We have used a new model of the large-scale gas distribution in the Galaxy, using a velocity-deconvolution of CO and H I line data that is based on self-consistently computed, non-circular gas flows in the inner Galaxy (Bissantz et al. 2003, Pohl et al. 2008, Englmaier et al. 2008). In contrast to many published studies, this model does not force azimuthal symmetry into the spiral-arm structure. The asymmetry of the arms near the solar circle erases any correlation to the 140-Myr cycle and any periodic trend less than the orbital period of our solar system relative to the spiral pattern as a whole. This would be greater than 500 Myr for the previously fit pattern speed. Even if we allow the pattern speed to vary, it will not be less than the orbital period of the Sun, which is still longer than the 140 Myr cycle in question. The asymmetry of the new galactic picture could create a correlation between the spiral arm crossings and any non-periodic event by

varying the pattern speed. We conclude that, based on these new data, there is no evidence to suggest any correlation between the transit of our solar system through the spiral arms of our Galaxy and the terrestrial climate.

3. Cosmic Ray Secondaries

Cosmic ray showers produce a large number of secondary particles through nuclear interactions in the atmosphere and media. These particles include protons, electrons, photons, and rare forms of matter such as pions and kaons. The large majority of secondaries continue to interact in the atmosphere, depositing their energy high above ground level. Particles with small interaction cross sections penetrate further in the atmosphere to ground level and below. The penetrating portion of the cosmic ray shower is known as the hard component and contains muons and neutrons. We focus on these particles as they contribute to ground level radiation as well as cosmogenic nuclide production.

3.1 Muons

Muons are created through the decay of charged pions in the atmosphere. These short lived, rare particles create biological effects on Earth at ground level. This is due to their high penetration which allows for a high flux at ground level (Cossairt & Elwyn 1987). Secondary cosmic rays are the dominant source of muons at ground level (Wissmann et al 2004). Cosmic Ray muons contribute significantly to the background radiation dose at ground level. This contribution will be greatly increased during a HECR event, impacting terrestrial biota (Atri & Melott 2011b). Solar events rarely contain

primaries of sufficient energy for muon production, and thus do not constitute a biological threat at ground level. The amount of radiation experienced by terrestrial biota is dependent on the total flux of cosmic rays as well as the spectral shape.

Figure 4 displays the differential muon flux at sea level due to three different scenarios: the current day cosmic ray flux, the galactic bow shock, and a nearby supernova. These results were tabulated using the lookup tables of Atri & Melott (2011a). These estimations use the cosmic ray flux of Medvedev & Melott (2007) for the galactic bow shock. The supernova cosmic ray flux is found by scaling the current day cosmic ray flux to supernova levels. This magnitude of this scaling is equal to the ratio of the current interstellar energy density to the energy density in the region of a nearby supernova. This energy density is approximated by dividing the total energy output of a typical supernova by the volume of a sphere of radius 10 pc. Under present day conditions, cosmic radiation comprises ~10-15% of the total radiation background. The majority of this radiation is attributed to cosmogenic muon flux. As this flux is increased by an order of magnitude during exposure to the galactic bow shock, this contribution becomes biologically threatening during such times (Atri & Melott 2011b). The cosmic ray flux generated by a nearby (<10 pc) supernova presents a much larger threat. The cosmogenic muon flux at sea level would be increased 2 or 3 orders of magnitude above the background. This level of radiation is known to be biologically damaging and is likely to produce a mass extinction. As muon flux is a form of penetrating radiation, these effects would not be confined to high altitude. Instead, the radiation dose due to a nearby supernova would extend to ground level and deep underwater and underground. Current supernova rate and

stellar density finds such an event statistically probable during the 500 Myr encompassed by the geologic record (Melott & Thomas 2011).

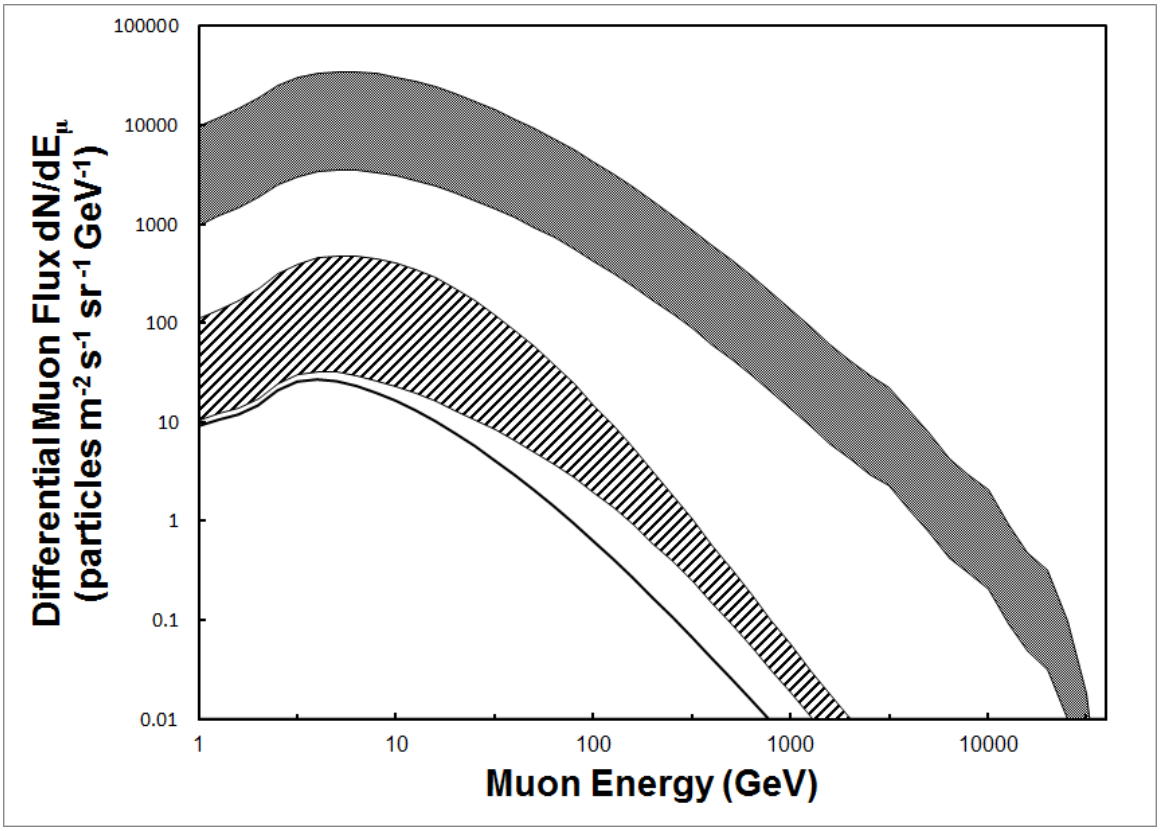

Figure 4: The solid line is the usual muon flux on the surface of the Earth. The striped band indicates the range of values in the extragalactic shock model, persisting for millions of years. The dark grey band indicates the range of possible enhancements likely when the Earth is closer than about 10 pc to a supernova. These flux levels, orders of magnitude higher than normal, would persist for a few hundred to thousand years.

3.2 Neutrons

Cosmogenic neutrons and their effects are a large area of research. This research includes atmospheric neutron measurements which have been taken since the 1950s at a variety of latitudes and altitudes (Davis 1950, Hess et al. 1959, Gordon et al. 2004, Goldhagen et al. 2004, Moser et al. 2005, among others). These measurements are useful for determination of cosmic ray flux variability. As these measurements span mere decades, they are inadequate for long term events such as the galactic bow shock of nearby supernova, and are primarily used to examine solar events. Solar proton events (SPEs) and the ground level enhancements (GLEs) of neutrons they produce are also if interest due to their effects on solid state devices (Duldig et al. 1994, Gordon et al. 2004, Gopalswamy et al. 2005, among others). An SPE is an energetic solar phenomenon which bombards the Earth with high energy protons. The upper limit on the energy of Solar SPEs is not known (Melott & Thomas 2012), though all SPEs contain sufficient energy for neutron production within our atmosphere (O'Brien et al. 1996).

Neutrons are formed through the process of cosmic ray spallation when high energy particles collide with atmospheric nuclei. Neutrons penetrate much further into our atmosphere than the electromagnetic component as they are not geomagnetically trapped. As they propagate, they collide with atmospheric nuclei, liberating additional particles as well as slowing to thermal energies (~0.025 eV). Once at thermal speeds these neutrons remain relatively stationary, with random motion due to their energy. Our work shows these thermal neutrons to be typically deposited in the stratosphere for lower

energy primaries, with higher energy primaries producing neutrons closer to ground level.

Neutrons constitute a source of cosmic radiation due to their high biological effectiveness (Reitz 1993). This radiation is a substantial risk factor in the stratosphere at high latitudes (Reitz 1993, O'Brien et al. 1996, Sigurdson & Ron 2004, Kojo et al 2005, Hammer et al. 2009, Beck 2009, among others). Cancer rates and rates of spontaneous abortion are increased significantly among flight crews (Pukkala et al. 1995, Aspholm et al. 1999). Variability in galactic cosmic ray flux has also been linked to increased cancer mortality and breast cancer (Juckett & Rosenberg 1997, Juckett 2007, Juckett 2009). A large HECR-created neutron flux at ground level would create widespread and devastating effects as the neutrons collide with nuclei contained within the biota. However, we find that the HECR increase needed to produce such a scenario would increase muon radiation by a substantially larger amount. For this reason, cosmogenic neutron radiation dose at sea level will always be less than the cosmogenic muon radiation dose from the same event. Despite this fact, cosmogenic neutrons still remain a threat at high altitude and the primary form of cosmogenic nuclide production.

Although solar events have been studied via neutron monitor measurements, no measurements exist for cosmic ray spectra produced by other astrophysical events. There is a non-trivial probability of events such as nearby supernovae (Erlykin & Wolfendale 2001, Fields et al. 2008) and gamma ray bursts (GRBs) (Dermer & Holmes 2005, Kusenko 2010, however see Abassi 2012) exposing the Earth to an enhanced flux of cosmic rays over Gyr timescales (Erlykin & Wolfendale 2010, Melott & Thomas 2011).

Motion of the sun perpendicular to the galactic plane has also been proposed to increase HECR flux due to increased exposure to the galactic shock (Medvedev & Melott 2007). These events are of substantially higher primary energy than SPEs, making them capable of producing devastating direct effects. Unlike other work which has focused on one case, the work we now share is applicable to any arbitrary HECR event, if the cosmic ray spectrum for the event is known. These events also produce high-energy photons which have been modeled in detail (Thomas et al. 2005, Ejzak et al. 2007) and will not be discussed further as we focus on cosmic ray effects.

3.2.1 Atmospheric Neutron Flux

Monte Carlo simulations have been performed for typical current cosmic ray fluxes, and have shown to reliably match atmospheric neutron measurements (Goldhagen et al. 2004, Grigoriev et al. 2010), however this work is limited to the current cosmic ray flux. Such work has been used to study ground level enhancements (GLEs) of neutron flux (Duldig et al. 1994, Gordon et al. 2004, Gopalswamy et al. 2005, among others). These enhancements are indicative of SPEs, and have been used to study their properties through the use of ground-based and atmospheric neutron monitors. Although this work is extensive, no work has been done to provide neutron fluxes independent of primary spectrum or for energies in the TeV range and above. For this reason we have tabulated neutron fluxes for a wide range of primary energies, independent of primary spectrum.

These results can be used to simulate the resulting neutron component in the shower from arbitrary cosmic ray spectra. Lookup tables represent proton primaries with energies ranging from 10^6 to 10^{15} eV. These energies, and other energies given in this paper, represent the kinetic energy of the particles. This is opposed to the total energy of the particle, which is used in high energy research groups and can be found by adding the mass energy of the proton (9.38272×10^8 eV) to our numbers. Protons comprise the large majority of cosmic rays and thus can be used as an approximation for all cosmic ray showers. This is done by approximating all primary nucleons as protons. Under this approximation, an alpha particle would be replaced with four protons. While under this approximation, results underestimate cosmic ray showers containing heavy nuclei. As other nuclei compose ~10% of cosmic ray primaries, this should be an adequate approximation despite the larger interaction cross section of heavy nuclei. Protons below 10^6 eV are not simulated in our work, as they do not create neutrons due to insufficient energy. This range (10^6-10^{15} eV) represents the largest portion of cosmic rays, and is therefore suitable for application to a wide range of astrophysical sources.

3.2.1.1 Computational Modeling

Computations were run as a two-step process. CORSIKA (COsmic Ray SImulations for KAscade) (Heck, 2001) was used for high energy interactions, while MCNP (Brown et al., 2002) and MCNPX (Pelowitz, 2005) were used for neutron

thermalization and propagation as well as low energy ranges. We calculated particle fluxes from single proton primaries, creating tables which can be used to deduce results from many different spectra.

CORSIKA is a Monte Carlo code used extensively to study air showers generated by primaries up to 100 EeV. It is well suited to high energy interactions, as it is calibrated using KASCADE, a detector used to study hadronic interactions in the 10^{16} to 10^{18} eV energy range, as well as with a number of other experiments around the globe. CORSIKA 6.960 was used for all high energy simulations. The code was set up with EPOS as the high-energy hadronic interaction model due to its compatibility with KASCADE data. The CURVED option was chosen for primaries incident at large zenith angles and the UPWARD option for albedo particles. The energy cut for the electromagnetic component was set at 300 MeV since it is adequate to get all the hadrons produced by photon interactions while saving a significant amount of computing time. The code was installed with the SLANT option to study the longitudinal shower development. This data is used to determine the neutron creation and propagation while above 50 MeV.

CORSIKA ignores neutrons with energies less than 50 MeV. To determine the propagation and thermalization of neutrons below this energy, we use MCNP. MCNP contains high resolution neutron cross sections which are superior to other similar Monte Carlo simulators (Hagmann et al. 2007). The longitudinal distribution of particles describes the location in the atmosphere where neutrons pass below 50 MeV. For each of these locations we simulated neutrons with kinetic energy of 50 MeV and angle equal to the primary angle. The atmosphere was modeled in ~100 bins corresponding to 10 g cm^{-2}

column depth each. The density and size of these bins were chosen using US Standard Atmosphere (1976). Flux tallies with order of magnitude neutron energy bins were set every 10 g cm^{-2} of column depth. Data obtained from the tallies of different angles at a given primary energy is then averaged by sin θ weight resulting in an isotropic spectrum at a particular primary energy. This weighted average is entered into the lookup tables for primary energies from 10 GeV – 1 PeV.

For the energy range 1 MeV – 10 GeV, MCNPX was used. MCNPX is the extended version of MCNP, allowing use at higher energies. MCNPX is better suited to lower energy interactions than CORSIKA, allowing for more reliable data. These simulations were performed in a way identical to the higher energy calculations, without the addition of the second step mentioned.

Identical simulations were performed using MCNPX for comparison in the energy overlap range from 1 GeV to 100 GeV. Within this range, the results of MCNPX were within statistical error of results from CORSIKA. This is consistent with other work showing comparisons between Monte Carlo simulations (Hagmann et al. 2007).

3.2.1.2 Results

Over the range of energies examined, the neutron production increases with primary energy (Figure 6). Our simulations show that the kinetic energy threshold for atmospheric neutron spallation is a few MeV. It should be noted that above the spallation

threshold, neutron production scales linearly with primary energy. With larger energy primaries, a larger portion of the energy will reach ground level, reducing neutron production efficiency. Additionally, high energy primaries lose much of their energy through inelastic collisions with nuclei which free additional neutrons. As the neutron production scales linearly with primary energy, the average neutron production is dependent on the average amount of energy deposited above production threshold in the atmosphere through cosmic ray interactions, and not on the high energy spectrum of the primaries.

Although the total neutron production does not significantly increase with primary energy, there is a large variation in the altitude at which the neutrons thermalize. High energy primaries produce more extensive showers freeing neutrons at lower altitudes. This creates the energy dependence of altitude distribution displayed in Figure 6.

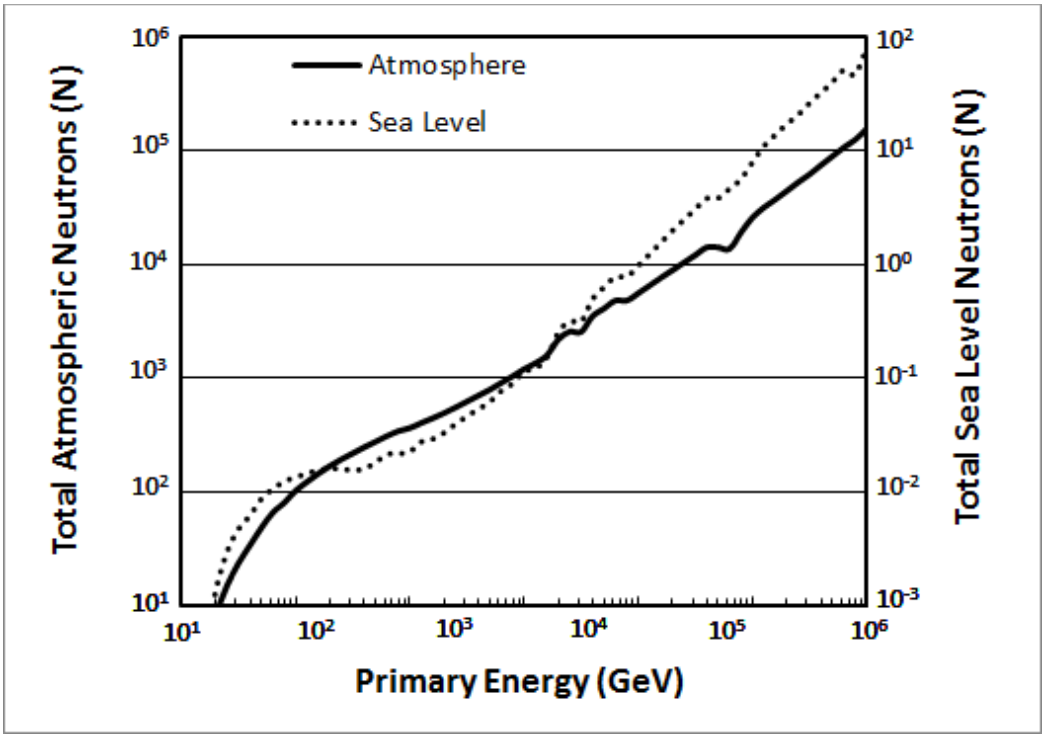

Figure 5: Number of neutrons produced in the atmosphere per primary as well as neutrons which reach sea level. Total atmospheric neutron number above sea level is plotted referencing the left-hand axis, with sea level neutron number referencing the right-hand axis. The shallower slope of the atmosphere line is due to higher energy primaries depositing more energy directly on the ground without producing neutrons in the atmosphere.

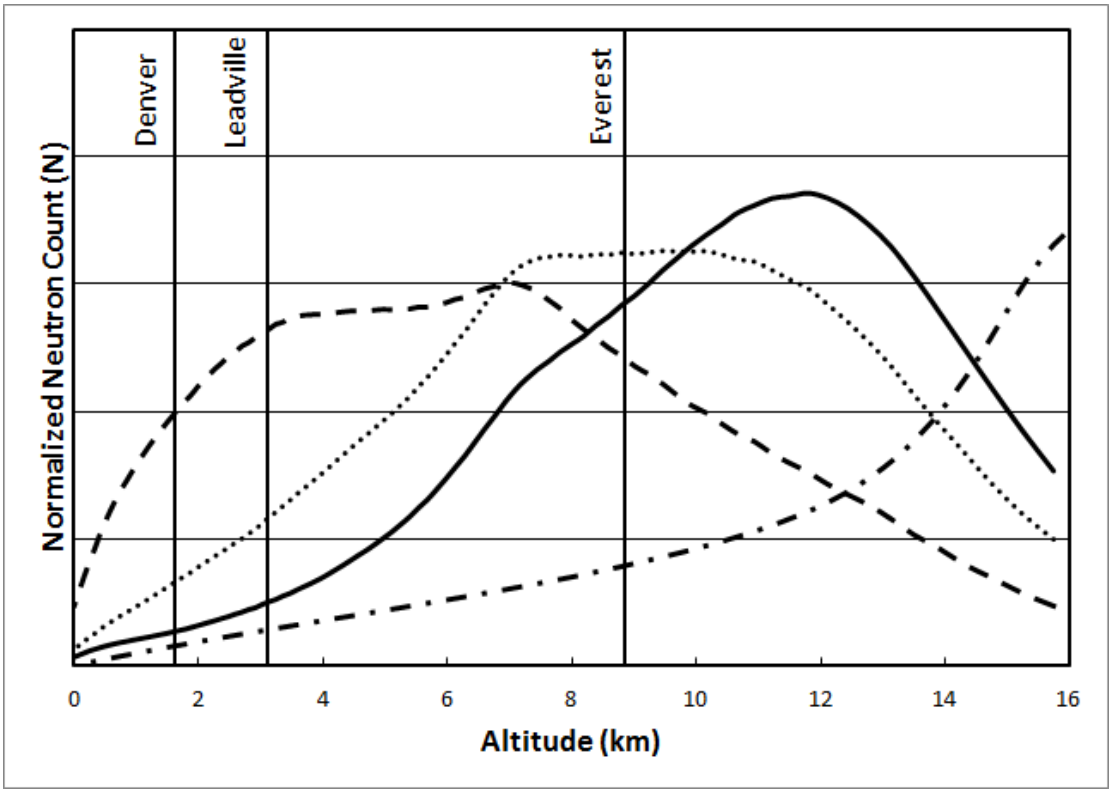

Figure 6: Normalized cosmic ray count per primary as a function of altitude above sea level. Neutron count is normalized by the total number of neutrons produced in the shower. The solid line represents a 10 GeV primary, with the dotted line representing 10 TeV primary, and dashed line representing 1 PeV primary. The present neutron distribution is given as a dash-dot line for comparison. Vertical lines correspond to commonly referenced altitudes: Denver, Colorado; Leadville, Colorado; and Mount Everest. High energy primaries produce neutrons at lower altitudes (See Figure 5) due to their secondaries having energies sufficient for further secondary production.

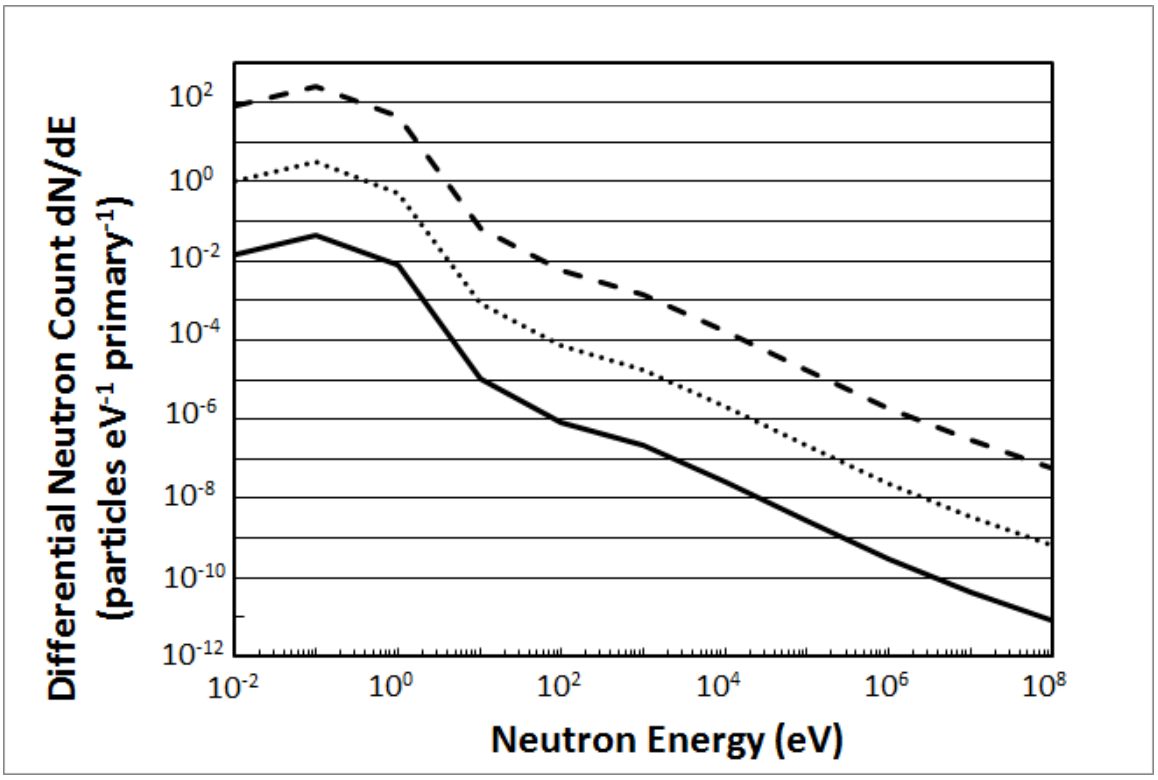

Figure 7: Differential neutron count at sea level as a function of neutron energy produced by 10 GeV (solid), 10 TeV (dotted), and 1 PeV (dashed) primaries. No neutrons reach ground level from primaries below ~1 GeV. Neutron energy is approximated with order of magnitude bins as with the table data. The spectral shape is similar for all energies due to the thermalization process.

Even though these factors greatly change the magnitude of the neutron flux, the terrestrial neutron spectrum remains generally invariant with respect to primary energy (Figure 7). This is to be expected due to the large number of collisions with atmospheric nuclei. Due to the invariance of the resultant spectral shape, it is probably impossible to derive the primary spectrum based solely on the neutron spectrum detected. This is consistent with the work of other researchers, which shows that neutron fluxes and GLEs scale to the magnitude of solar events, but not the spectra of individual events (Plainaki et al. 2007).

3.2.1.3 Using the Lookup Tables

The lookup tables are organized three different ways: by primary kinetic energy, by column density, and by neutron energy. Each set contains a number of tables equal to the number of bins of that variable; 91, 94, and 10 respectively. Results display the number of neutrons per eV for a given bin. Primary kinetic energy is divided into 10 logarithmic bins per order of magnitude and labeled with units log eV (2 corresponding to 10^2 eV, etc.). Column density is given in units of g cm^{-2} with bins of size 10 g cm^{-2}. There are ten neutron energy bins, with labels of units log eV. Primary spectra from astrophysical sources often contain units of particles GeV^{-1} m^{-2} sr^{-1} s^{-1}. The number of neutrons can be calculated using such a spectrum by multiplying the primary spectrum by the corresponding table values and summing over the desired primary kinetic energy and

neutron energy bins. The total neutron flux can be found by multiplying these individual results by their corresponding bin size before summing.

Statistical and systematic errors were calculated for our results. Statistical errors vary depending on bin size, however in all cases the standard deviation of the mean is less than 10% of the total bin value. These errors are concentrated in regions of low neutron number, making results near the neutron production threshold the least well known. Systematic error is introduced through latitude, geomagnetic and seasonal variation. These effects can be corrected for by modulating the primary spectrum before convolution. With a properly modulated cosmic ray spectrum, systematic errors are dominated by the use of proton exclusive simulations. As cosmic rays contain heavier nuclei, results will underestimate neutron production. Most of this error can be eliminated by use of a primary spectrum in units of particles GeV^{-1} m^{-2} sr^{-1} s^{-1} $nucleon^{-1}$. For these purposes, alphas, the second-dominant species in cosmic ray shower, will count as four particles each. In such a situation, this should reduce the systematic error to inconsequentiality in comparison to statistical error. Although systematic errors from heavy nuclei are in principle unknown due to unknown cross sections, they prove to be small using this approximation as table results are found to match neutron monitor measurements. Our results have been tested against the neutron monitor measurements of Goldhagen et al. (2004). Using the "particles" count, our results match well to these measurements, as both display the same two peaked neutron spectrum shape, and the flux of neutrons < 10 MeV agree to better than 20%. Our tables are independent of latitude

and are produced with the average cosmic ray background. These approximations and statistical errors account for the discrepancy.

3.2.1.4 Discussion

Cosmic ray induced neutron flux remains a threat to airplane flight crews, especially at high latitude and altitude. In the event of an increased HECR flux, effects would be prevalent at lower altitudes. These effects would be very small at ground level in most cases. Any event of energy sufficient for producing large ground level neutron radiation will be accompanied by a greatly increased and more penetrating muon flux (Atri & Melott, 2011a). For this reason, ground level cosmic ray secondary radiation will always be dominated by its muonic component. Events such as supernovae and gamma ray bursts (However, see Abassi 2012) could increase the HECR flux for an extended period of time, instigating or encouraging a mass extinction. Increased cosmic rays for several Myr could account for mass extinction periodicity if the HECR flux were increased periodically. A periodicity in biodiversity has been shown to exist within the fossil record (Melott & Bambach 2011), with the driving mechanism still unknown (However, see Melott et al. 2012). Our results show neutron radiation doses to be small in comparison to muon radiation dose at ground level. Even a large SPE, such as the Carrington event of 1859, would only increase the neutron flux by ~ 5%. This remains very small in comparison to muon radiation dose during the same period. HECR events,

with their harder spectra, will always increase muon flux by a greater amount than neutron flux. Although neutrons have little biological impact at ground level, they remain a threat at higher altitudes. Additionally, the soft error rate of solid state devices is affected by cosmic ray induced neutrons as well. As no simple method has existed for calculation of HECR induced neutron flux, we have developed lookup tables that can be used for primaries ranging from 1 MeV – 1 PeV. Radiation dose can be calculated from these tables using appropriate biological effectiveness. Data is made freely available at: http://kusmos.phsx.ku.edu/~melott/crtables.htm .

4. Cosmogenic Nuclide Production

Rare and common nuclides are continuously produced by cosmic rays in the Earth's atmosphere and other regions bombarded by cosmic rays. These nuclides are produced when cosmic ray primaries and secondaries collide with target nuclei. The subsequent nuclear reactions produce nuclides which often remain within the target material before decaying some time later. Although many secondary particles are capable of such reactions, neutrons are the dominant source of cosmogenic nuclides.

Cosmogenic neutrons are the fundamental source of nuclide production both within Earth's atmosphere and in other target matter. This nuclide production is very well studied and production rates have been measured (Lal 1991, Masarik & Reedy 1995, Masarik & Beer 1999, among others). Two different forms of interaction are responsible for nuclide production from neutrons: spallation and thermal neutron absorption. Spallation is the fragmentation of target nuclei by high energy neutrons. These interactions free neutrons and protons from the nucleus, thereby changing the composition of the target nucleus. Neutrons which are slowed to very low energies (<0.025 eV) are referred to as thermal neutrons. These neutrons can be absorbed into target nuclei, thereby altering the composition of the nucleus. The interaction cross section for these interactions is largely target dependent.

Of the many cosmogenic nuclides produced in cosmic ray showers, our work focuses on three particular isotopes: ^{14}C, ^{10}Be, and ^{26}Al. We focus on these isotopes as they are among the most abundant produced in our atmosphere, they are well measured in

ice cores, and their production efficiency varies from the atmosphere to extraterrestrial matter.

4.1 In the Atmosphere

The atmosphere is the largest source of cosmogenic nuclide production on the Earth. These nuclides are produced during cosmic ray showers when neutrons and other secondaries interact with atmospheric target nuclei. The most common cosmogenic nuclide within the Earth's atmosphere is ^{14}C, however other examples exist such as ^{26}Al, ^{10}Be, and ^{36}Cl.

^{14}C is predominantly produced in our atmosphere when thermal neutrons are absorbed into ^{14}N nuclei. Most of this absorption occurs at high latitudes and altitudes due to low energy cosmic rays. This absorption creates an excited, unstable version of the isotope ^{15}N referred to as a metastable state or isomer, which quickly decays into ^{14}C by ejecting a proton through the process:

$$^{1}\mathrm{n} + {}^{14}\mathrm{N} \rightarrow {}^{14}\mathrm{C} + {}^{1}\mathrm{p}, \qquad (1)$$

Other possible production mechanisms include the spallation of larger nuclei. Some ^{14}C is therefore created through the spallation of ^{16}O in the process:

$$^{1}n + {}^{16}O \rightarrow {}^{14}C + {}^{1}n + \alpha, \qquad (2)$$

or similar reactions of the form ^{16}O(t, 5u)^{14}C. This radiocarbon, as it is called, often joins atmospheric oxygen to form carbon dioxide. Atmospheric carbon dioxide is absorbed into plants, the ocean, and other carbon sinks; thereby distributing ^{14}C within these different reservoirs. The largest of these reservoirs is the ocean, where the majority of radiocarbon is found. Despite these effects, large amounts of radiocarbon remain in our atmosphere. Tree rings and ice cores have been used to give a record of past radiocarbon concentrations within our atmosphere (Stuiver et al. 1998, Hua et al. 2009, Miyake et al. 2012, among others). Although the radiocarbon production rate is generally invariant, deviations from this state exist within the record. These deviations are evidence of variance in terrestrial cosmic ray flux, changes in ocean circulation, and possibly impacts from extraterrestrial objects.

Other cosmogenic nuclides are produced in the Earth's atmosphere in measurable amounts, such as ^{26}Al and ^{10}Be. Although these nuclides are rarer than radiocarbon in our atmosphere, some can still be detected in ice cores. ^{10}Be and ^{26}Al have been measured in ice cores in both Greenland and Antarctica (Finkel & Nishiizumi 1997, Auer et al. 2009). As these two isotopes precipitate out of the atmosphere without being absorbed by the ocean, their atmospheric concentration is less dependent on ocean circulation. Comparisons of these isotopes can give additional information on the nature of cosmogenic nuclide variances detected in the geologic record.

^{10}Be is produced in our atmosphere by spallation of atmospheric nuclei. Typical spallation processes are of the form ^{14}N(t, 5u)^{10}Be, such as:

$$^{1}n + {}^{14}N \rightarrow {}^{10}Be + {}^{1}n + \alpha$$

however other examples exist. These interactions are common due to the large number of atmospheric nuclei with sufficient nucleons for ^{10}Be creation.

The majority of ^{26}Al produced in our atmosphere occurs from spallation of ^{40}Ar by high energy cosmic rays in the process ^{40}Ar(p, sp)^{26}Al. As this occurs in a single isotope and is largely dependent on cosmic ray energy, ^{26}Al remains to be a rare isotope in the Earth's atmosphere. Although ^{26}Al is produced more efficiently through the spallation of silicon, there is not enough precursor silicon within the Earth's atmosphere to make this the predominant source of ^{26}Al on Earth. This contrasts the production on extraterrestrial matter, where the contribution from silicon spallation far outweighs argon spallation. For this reason, a much greater amount of ^{26}Al is produced on extraterrestrial matter than in the atmosphere under the same conditions.

4.2 On Comets and Meteors

Comets and meteors spend the majority of their lives outside the protection of the magnetosphere of the Earth and possibly the heliosphere. These locations are continually bombarded by a much greater flux of cosmic rays. For this reason, cosmogenic nuclides are produced at much higher rates than in the Earth's atmosphere. Their lack of atmosphere exposes a wide range of nuclei which are not exposed on the Earth. These two factors increase certain nuclide production rates far above terrestrial levels. A large comet or meteor can contain a measurable amount of certain cosmogenic nuclides even when distributed throughout the Earth's atmosphere. As these nuclides are detected in the geologic record, these measurements may provide clues to past impact events.

Impacts from extraterrestrial objects provide a significant threat over long timescales of damage and mass extinction for terrestrial biological systems. As well as directly damaging biological systems, extraterrestrial impacts are known to create long-lived atmospheric effects, such as ash and dust clouds. Little is known of the frequency of such events, and what is known depends greatly on cratering and other geologic data (Raup & Sepkoski 1984, Bland et al. 1998, Jetsu 2011) which do not measure airbursts. The extinction event at the end of the Cretaceous period (KPg boundary) coincides with a large bolide impact proposed to be the primary cause of the extinction event (Alvarez et al. 1980).

Impact events are produced by a variety of extraterrestrial objects, including iron meteorites, rocky asteroids, and icy comets. Meteorites are well studied, because they typically leave craters and residual fragments of the initial object. In other cases, the impactor can break up in an airburst when rapid thermal expansion of the object produces fracturing and an apparent explosion of the nucleus before reaching ground level. These events are more difficult to study and leave less evidence than terrestrial impacts, making their frequency largely unknown. Major airbursts release a large amount of energy that may threaten biological systems, as an example, during the Tunguska event, which occurred above Siberia in 1908 (Farinella et al. 2001). The mass of the Tunguska cosmic body is estimated to have been $5x10^7$ kg (Wasson 2003); it produced the largest airburst in recorded history and felled an estimated 80 million trees. A similar, smaller event was recorded in 2013 over Chelyabinsk, Russia. The bolide for this event has been estimated to have a mass of ~10^7 kg. An event much larger than Tunguska has been suggested as the possible cause of the Younger Dryas cooling event of the late Pleistocene. Reported evidence for this impact includes peaks in microspherules, high-temperature melt-glass (>2100°C), iridium, osmium (Sharma et al. 2009), polycyclic aromatic hydrocarbons, and nanodiamonds (Firestone et al. 2007, Kurbatov 2010, Israde-Alcantaraz 2012, Bunch et al. 2012), all of which are also present in the KPg boundary layer. The impactor for this event was conjectured to be a 1-4+ km wide comet, making this event many orders of magnitude larger than Tunguska (Bunch et al. 2012). However, this hypothesis and the origin of the reported evidence are still controversial (Kerr 2008, Surovell et al. 2009, but

see Lecompte et al. 2012). In this paper, we do not address this controversy, but rather whether or not the nuclide evidence is consistent with causation by a large impact.

4.2.1 Long-Period Comets

Long-period comets present a unique threat due to their relative unpredictability (Napier & Asher 2009). These comets often begin in the Oort cloud, a spherical arrangement of extraterrestrial ice and dust ~50,000 AU from our sun; from there, they may be perturbed from orbit and fall towards the center of our solar system. This cloud resides within the interstellar medium (ISM), an environment vastly different from the inner solar system. With very little direct measurement data available for these comets, their cosmogenic nuclide abundances remain unknown.

Comets and other bolides entering Earth's atmosphere will deposit detectable residue, as occurred when the KPg boundary impactor deposited a worldwide layer of iridium that was used as a primary argument for its existence (Alvarez et al. 1980, Shulte et al. 2010). Melott et al. (2010) showed that cometary airbursts may deposit nitrates and ammonium potentially detectable in ice core data, and these are consistent with data for the Tunguska event. If excess cosmogenic isotopes exist in comets due to increased cosmic ray exposure prior to their impact, then comets may also deposit these in the atmosphere, causing a deviation from background abundances in the record. However, because other processes, such as geomagnetic changes or sudden fluctuations in ISM

cosmic-ray flux (Erlykin & Wolfendale 2010) can also produce isotopic excursions, increases in such nuclides alone cannot be counted as evidence of an impactor. On the other hand, extraterrestrial matter produces cosmogenic nuclides in different proportions than that of cosmic ray showers in Earth's atmosphere, and therefore, variance in the ratios of cosmogenic nuclides can potentially provide evidence for past impact events. In particular, we show one such ratio to be a good test for the Younger Dryas impact hypothesis.

4.2.1.1 Comet Composition

In order to compute the expected cosmogenic isotope production on a comet, we make assumptions about its composition, which varies greatly depending on the origin and history of the comet. The comet nucleus (often called a "dirty snowball" or "icy dust ball" depending upon composition) contains rock, frozen gases, and a large amount of water ice combined with ices of other volatiles. The densities of most short-period comet nuclei vary from 0.3 to 0.6 g/cm^3 (Britt et al. 2006), whereas the density of long-period comets are probably lower, but largely unknown due to limited measurement opportunities.

Cosmogenic nuclide production occurs when high energy particles collide with atomic nuclei, and these collisions produce secondary particles of varying types in cascades known as a particle showers. Important secondary particles include protons,

neutrons, and pions. A large variety of nuclides can be produced in the case of large target nuclei (Michel et al. 1997), making the presence of abundant target elements within long-period comets important. Comets are composed of roughly equal parts ice and dust. Hydrogen, oxygen, nitrogen and carbon are the most abundant elements in cometary ice, while oxygen, carbon and silicon are the most abundant elements in cometary dust. We focus on the most commonly measured cosmogenic nuclides ^{10}Be, ^{14}C, and ^{26}Al, which are produced in collisions with carbon, silicon, oxygen and nitrogen. ^{10}Be and ^{14}C are the most abundant cosmogenic isotopes in the Earth's atmosphere. ^{14}C has been measured in tree rings and ice cores, while ^{10}Be has been measured in ice cores, developing a record of atmospheric abundance for these two isotopes. Production of ^{10}Be is caused by the direct spallation of oxygen and nitrogen and ^{14}C is also produced by the absorption of cosmic ray neutrons by nitrogen. Extensive measurements have been made on the composition of Halley's comet, in particular for its nitrogen content; the N/O ratio within Halley was found to be 0.047 within the dust and 0.023 overall (Wyckoff et al. 1991), far below solar levels. This nitrogen is found as ammonia and in organic molecules. ^{26}Al is produced at high efficiency in extraterrestrial matter, because of the direct exposure of the silicon in comets or asteroids to cosmic rays. On the other hand, terrestrial production of ^{26}Al is low because very few cosmic rays reach the ground, with the result that most terrestrial production is confined to the atmosphere, where silicon abundance is low. ^{36}Cl is another well studied cosmogenic nuclide derived from argon. However, with very little precursor argon present in cometary matter, its production should be negligible.

On their first entrance into the inner solar system, comets contain a large fraction of volatiles. These volatiles (such as ammonia) remain frozen in the comet nucleus while the comet is sufficiently far from the Sun, as in the Oort cloud, but, while on approach, the surface temperature of the comet nucleus is raised through radiant heating to the point of sublimation of these frozen volatiles. As a large portion of cometary nitrogen is found in frozen and gaseous ammonia, long-period comets and comets on first approach contain fractionally higher amounts of nitrogen. For this reason, we will assume the Halley nitrogen ratio as a lower bound; this nitrogen abundance lies well below solar values (Krankowsky 1991, Wyckoff et al. 1991). In addition to nitrogen depletion through outgassing, depletion is also thought to occur during the creation of comets (Iro et al. 2003). Objects originating in low-temperature environments, such as long-period comets from the Oort cloud, may contain more nitrogen than other comets, consistent with solar abundances (Owen 2003). Measurements of distant comets within the heliosphere show higher nitrogen abundances (Korsun et al. 2008). Therefore, we use solar nitrogen abundances as an upper bound.

4.2.1.2 Cosmic Ray Environment

Current terrestrial cosmic ray flux is well measured and known, but is not so well known outside the protection of the Earth's magnetosphere, where long-period comets originate. Measurements of the cosmic ray flux in interplanetary space have been taken

by the Voyager space probes since launch (Stone et al. 1977), but the probes have yet to completely exit the protection of the Sun's magnetic field. Even so, Voyager is currently entering the interstellar medium and it provides important measurements that serve as benchmarks in choosing a cosmic ray spectrum. The cosmic ray flux of interplanetary space is greater than terrestrial levels, and the flux is also expected to be greater beyond the heliosphere. Many models have been proposed for describing this spectrum (e.g. Spitzer & Tomasko 1968, Hayakawa et al. 1961, Nath & Biermann 1994, Mori 1997, Valle et al. 2002, Kneller et al. 2003, Herbst & Cuppen 2006, Indriolo et al. 2009). Most of these models are now eliminated as the Voyager probe has already detected cosmic ray fluxes in excess of their predictions. The plausible models are those which contain cosmic ray fluxes equal to or exceeding the latest Voyager results. This criterion selects the cosmic ray spectra of Hayakawa et al. (1961) and Nath & Biermann (1994) as most reasonable.

Models consistent with Voyager measurements greatly exceed terrestrial cosmic ray fluxes. For cosmic rays with energies sufficient for magnetosphere penetration (~10 GeV), the interplanetary and interstellar cosmic ray spectrum remains little changed from the terrestrial level. However, in energy ranges below this, the cosmic ray flux is increased by many orders of magnitude. Of special interest to our work are cosmic rays in the range from 10 MeV – 1 GeV, which are increased 3 to 5 orders of magnitude outside the heliosphere and are also above the threshold for producing cosmogenic nuclides. In particular, cosmic rays of this energy produce abundant secondary neutrons in particle

showers, as well as ^{10}Be and ^{26}Al through spallation (Lange et al. 1995, Michel et al. 1997).

We model long-period comets as spheres with the composition specified above which spend their lifetime outside the heliopause, before a perturbation sends them into the inner Solar System.

4.2.1.3 Cosmogenic Nuclide Production

The isotope produced in largest quantities in our atmosphere is ^{14}C, created by the absorption of cosmic ray produced neutrons by ^{14}N. Production of ^{10}Be is caused by the direct spallation of nitrogen and oxygen by protons and neutrons. ^{26}Al is produced primarily through the spallation of silicon, but other heavy target nuclei produce this isotope as well.

We have performed Monte Carlo simulations using MCNPX 2.6 (Hendicks et al. 2007) which is optimized for neutron transport. Monte Carlo simulators such as MCNPX are extensive programs based on all fundamental interactions with elementary particles, and they are often used for simulation of cosmic ray showers and other high energy interactions. MCNPX has been used to simulate cosmic ray showers in both the atmosphere and in spallation neutron producers. For our simulation, a comet was modeled as a column of ice and dust best fitting what is known of comet nucleus density and composition. It was given a length sufficient for inclusion of all cosmic ray

secondaries and periodic boundary conditions. Column composition consisted of equal parts ice and dust, matching the elemental abundances of Halley. Elemental abundances within the ice were chosen to be ~11% hydrogen, ~79% oxygen, ~4% nitrogen, and ~6% carbon by mass (Delsemme 1982). While the dust abundances were chosen to be ~5% hydrogen, ~24% carbon, ~1.5% nitrogen, ~35% oxygen, ~0.6% sodium, ~6% magnesium, ~0.5% aluminum, ~13% silicon, ~6% sulfur, ~0.02% potassium, ~0.6% calcium, ~0.05% titanium, ~0.1% chromium, ~0.07% manganese, ~7% iron, ~0.04% cobalt, ~0.6% nickel (Jessberger et al. 1988). As the density and composition of long-period comets is only partially known, a larger fraction of volatiles was tested in simulations with very little impact on secondary production.

Models were run at 10 logarithmic primary kinetic energies between 10 MeV and 1 GeV, and in order of magnitude bins above 1 GeV. Output was given in the form of cell average flux tallies, including proton and neutron cell average fluxes in 100 logarithmic energy bins. These tallies produce secondary proton and neutron fluxes per primary, which were then convolved with the cosmic ray spectrum to produce total proton and neutron fluxes. As expected, neutron production rates inside the comet were found to exceed atmospheric rates. This is due to the increased density of comet matter, giving secondaries additional interaction opportunities before their decay or absorption.

Convolution of the acceptable cosmic ray spectra with the individual neutron production rates produced a total neutron flux. This neutron flux was multiplied by the absorption cross section for the nitrogen content within the nucleus to find the rate of ^{14}C production in the comet. ^{14}C is radioactive with a half-life of 5730 years (Godwin 1962).

The amount of ^{14}C on the comet at any given time is therefore that sustainable at steady state between production and decay. As we are considering long-period comets, this will provide a very good approximation for the ^{14}C residing on the comet at any given time. This is because a long-period will spend at most 200 years, a negligible portion of its lifetime, in its first entrance into the heliosphere, which is insufficient for a significant decay of these cosmogenic nuclides. This amount was found by equating the production rate and the decay rate on the comet. We calculated this amount within 20 depth bins of one meter each as follows:

$$m_C \lambda_C = \int \Phi(m, E, r) \sigma_C(m, E)\, dr\, dE, \qquad (1)$$

where m_C is the mass of ^{14}C on the comet, λ_C is the decay constant of ^{14}C (0.00012 yr^{-1}), Φ is the flux of neutrons in the comet, and σ_C is the total interaction cross section for ^{14}C production. Both the flux of particles and the interaction cross section will depend on the mass of the comet and the energy of the particles interacting with the comet. The flux of secondary particles depends strongly on the depth of the comet (r) and is reduced to negligibility beyond a depth of ~20 m. This is consistent with atmospheric measurements, as the column density of cometary matter at 20 m is equivalent to the column density of the atmosphere at sea level. Integration was done numerically for 20 depth bins of 1 meter each, and 10 order of magnitude neutron energy bins.

The comet will reach this steady state amount during its residence in the interstellar medium (short-period comet rates can be estimated as two orders of

magnitude lower). The steady state amount will depend on the cosmic ray spectrum chosen. We have chosen the cosmic ray spectra of Hayakawa et al. (1961) and Nath & Biermann (1994), which produce the range of cosmogenic nuclide production displayed in our results.

^{10}Be is produced through the spallation of oxygen and nitrogen. The interaction cross section for this process has been well studied for a variety of primary energy ranges (Lange et al. 1994, Michel et al. 2007, Kovaltsov & Usoskin 2010). To find the rate of ^{10}Be production, we multiplied the proton and neutron fluxes by their corresponding total interaction cross sections. ^{10}Be is radioactive with a half-life of 1.387 Myr. To find the amount of ^{10}Be present on the comet at any given time, we set the production rate in interstellar medium equal to the decay rate on the comet. This creates a steady state equation similar to that for ^{14}C:

$$m_{Be}\lambda_{Be} = \sum_i\left(\int \Phi_i(m, E, r)\sigma_{i,Be}(m, E)\ dr\ dE\right), \qquad (2)$$

where m_{Be} is the mass of ^{10}Be on the comet, λ_{Be} is the decay constant of ^{10}Be (~$5x10^{-7}$ yr^{-1}), Φ_i is the flux of high energy particles in the comet, and $\sigma_{i,Be}$ is the total interaction cross section for ^{10}Be production for particle type i. The flux of high energy particles behaves similarly to the flux of neutrons in equation (1). Numerical integration was used with bins similar to equation (1).

^{26}Al is produced through the spallation of many heavy isotopes, primarily silicon. The interaction cross section for this process has been well studied for a variety of

primary energy ranges (Lange et al. 1994, Michel et al. 2007, Kovaltsov & Usoskin 2010). To find the rate of ^{26}Al production, we multiplied the proton and neutron fluxes by their corresponding total interaction cross sections. ^{26}Al is radioactive with a half-life of 717 kyr. To find the amount of ^{26}Al present on the comet at any given time, we set the production rate in interstellar medium equal to the decay rate on the comet. This creates a steady state equation similar to the ^{14}C and ^{10}Be versions:

$$m_{Al}\lambda_{Al} = \sum_i\left(\int \Phi_i(m, E, r)\sigma_{i,Al}(m, E)\, dr\, dE\right), \qquad (3)$$

where variables are named in analogy to equations (1) and (2), and λ_{Al}~9.7×10^{-7} yr^{-1}.

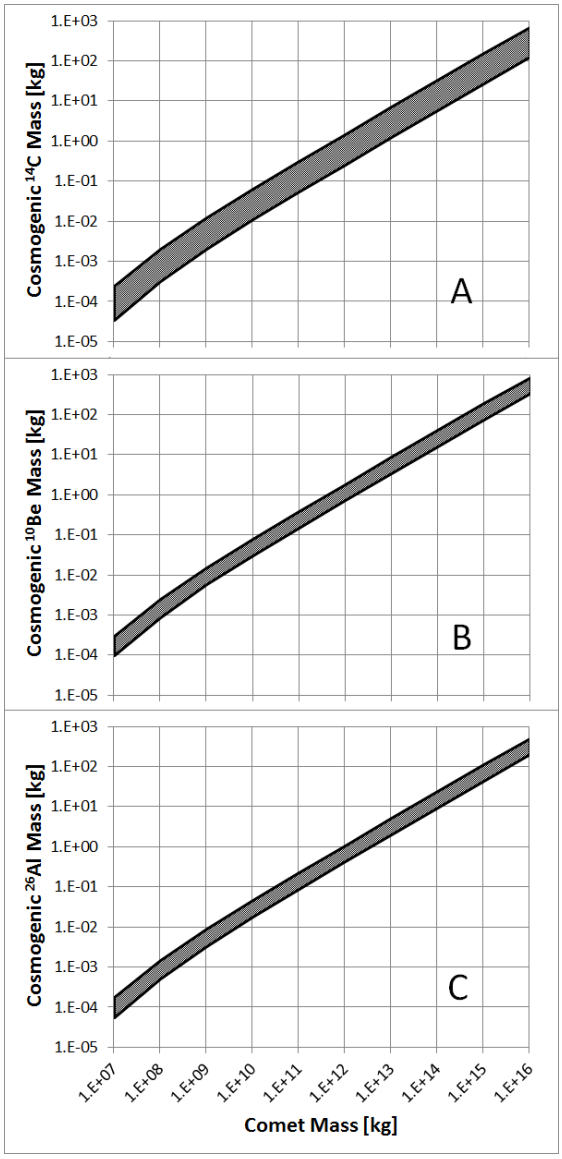

Figure 8: Cosmogenic ^{10}Be, ^{14}C, and ^{26}Al mass contained on a long-period comet as a function of comet mass. Shaded regions designate uncertainty based on interstellar medium cosmic ray spectrum, comet density, and composition. Figure 1A corresponds to cosmogenic carbon, Figure 1B corresponds to cosmogenic beryllium and Figure 1C corresponds to cosmogenic aluminum. All axes are plotted logarithmically.

4.2.1.4 Results

4.2.1.4.1 Cosmogenic Carbon-14

Comet ^{14}C abundance has been calculated for comets ranging in size from 10^7 to 10^{16} kg. Figure 1A shows ^{14}C mass as a function of total comet mass. For this figure, we assume a spherical comet of density between 0.3 g/cm^3 and 0.6 g/cm^3, and the elemental abundances of Halley as well as solar abundances. The lower bound corresponds to a density of 0.6 g/cm^3 and the nitrogen abundance of Halley; the upper bound corresponds to a density of 0.3 g/cm^3 and solar nitrogen abundance. This range includes all comet compositions which have been measured.

Any comet small enough to allow secondaries to exit without interaction is also too low in mass to have a measurable impact on the cosmogenic nuclide abundance of the atmosphere. This is due to the secondary neutron flux decreasing to nil after ~20 meters. This makes the mass of cosmogenic nuclide in the relevant mass range go roughly as the surface area, or $m_c^{2/3}$ for a spherical object.

As shown in Figure 8A, the amount of mass deposited in the case of small comets is insignificant compared with the average ^{14}C mass in the atmosphere, or approximately 500 kg. To make a noticeable change to the ^{14}C record, an impactor must contain ~1% of this total mass, or ~5 kg. This makes the detection of impactors in ^{14}C only plausible in the case of very large objects which reside primarily outside of the heliosphere. Impact events from such objects are decidedly rare but pose a significant threat to life. Short-

period comets and other extraterrestrial objects which orbit primarily within the heliosphere would have cosmogenic nuclide masses almost two orders of magnitude smaller, so they will not be likely candidates for significant ^{14}C or ^{10}Be enhancement.

4.2.1.4.2 Cosmogenic Beryllium

Comet ^{10}Be abundance has been calculated for comets ranging in size from 10^7 to10^{16} kg. Figure 8B displays ^{10}Be mass as a function of comet mass. We again assume a spherical comet of density between 0.3 g/cm^3 and 0.6 g/cm^3. A nonspherical cometary nucleus would produce somewhat higher amounts of cosmogenic isotopes.

These results can be compared to experimental results from carbonaceous chondrites. Carbonaceous chondrites are stony meteorites which were tested (Goel 1969) for the presence of ^{10}Be. The ^{10}Be concentration was found to be roughly twice what our results show for long-period comets. This difference arises from the lower abundance of (primarily oxygen) target nuclei to create ^{10}Be on comets, as well as a smaller fraction of comet mass lying within the spallation zone. Although these chondrites are capable of producing cosmogenic nuclides such as ^{10}Be, they lack the nitrogen content to produce measurable ^{14}C atmospheric enhancements.

The ^{10}Be content shown in Figure 8B is large in comparison to present day ice core concentrations. However, as in the case of ^{14}C, this amount depends greatly on the trajectory and mass of the extraterrestrial object. Unlike ^{14}C, ^{10}Be does not depend as heavily on target nitrogen, and thus, provides little information on composition of the

extraterrestrial object. Also unlike ^{14}C, the processes by which ^{10}Be is deposited into ice cores are dependent on a larger variety of factors, such as snowfall rates and circulation of ^{10}Be within the atmosphere (Finkel & Nishiizumi 1997). This makes ^{10}Be ice core abundance less dependent on atmospheric abundance, where cometary ^{10}Be would be deposited.

4.2.1.4.3 Cosmogenic Aluminum

Comet ^{26}Al abundance has been calculated for comets ranging in size from 10^7 to 10^{16} kg. Figure 8C displays ^{26}Al mass as a function of comet mass. These results are consistent with measurements of other extraterrestrial matter (Nishiizumi et al. 1995).

The production of ^{26}Al is greatly enhanced compared to terrestrial levels. This enhancement is caused by substantially larger amounts of silicon being present on the surface of the comet. On the Earth, most of the silicon lies under the protection of a fairly thick atmosphere, allowing very little ^{26}Al production. Our results show the mass of ^{26}Al to be near to that of ^{10}Be. As the deposition processes of ^{26}Al are very similar to those of ^{10}Be, the ratio of $^{26}Al/^{10}Be$ in the ice core would reflect the effect of the ratio on the bolide at the time of deposition. This ratio escapes the uncertainty in deposition processes, making it more dependent on presence of cometary matter in our atmosphere than either one of these isotopes alone.

4.2.1.5 Discussion

Our results show that measurable amounts of ^{14}C will be deposited in our atmosphere by large long-period comets. Short-period comets can be expected to contain two orders of magnitude less ^{14}C, making them impossible to measure except in bolides larger than ~$5x10^{15}$ kg. Long period comets equal to the catalog average mass should contain a measurable amount of ^{14}C, up to ~5% of the total atmospheric ^{14}C or greater, as in the case of a large comet such as Halley. This amount scales as $m_c^{2/3}$, due to the surface area of the comet.

The Tunguska event remains a benchmark for recent bolide impacts, and our work is based on the current estimated $5x10^7$ kg mass of the Tunguska object (Wasson 2003). If the Tunguska impactor were a long-period comet with half its mass in volatiles, the amount of ^{14}C produced would still be minimal and well below measurable amounts, consistent with measurements at that time (Stuiver et al. 1998).

The hypothetical Younger Dryas object is proposed to have been an object with a mass between $4x10^{12}$ kg (Bunch et al. 2012) and $5x10^{13}$ kg (estimated by Toon et al. 1997 as sufficient for continent-wide devastation). Given this range, the object could have deposited ^{14}C between ~0.5% and ~6% of total atmospheric ^{14}C. This is sufficient to explain the ~5% ^{14}C increase measured at the onset of the Younger Dryas event, which has been observed in tree rings (Hua et al. 2009), ice cores (Stuiver et al. 1998), lake sediments (Ramsey et al. 2012), and ocean sediments (Hughen et al. 2006), as shown in Figure 9. This increase would require a very large mass comet with low density. Impacts

of this size are rare. At a rate of 10^{-6} per year, admittedly dominated by small-number statistics (Chapman & Morrison 1994), the probability of one in the last 13,000 years is close to 1%. However (Asher et al. 2005, Napier & Asher 2009) suggest that the rate is much higher, particularly for long-period comet impacts. Although changes in ocean circulation are proposed to affect the ^{14}C concentration in this record, research suggests that this is not the case (Muscheler et al. 2000). Our results provide an alternative possibility for this deposition, which is currently not well understood.

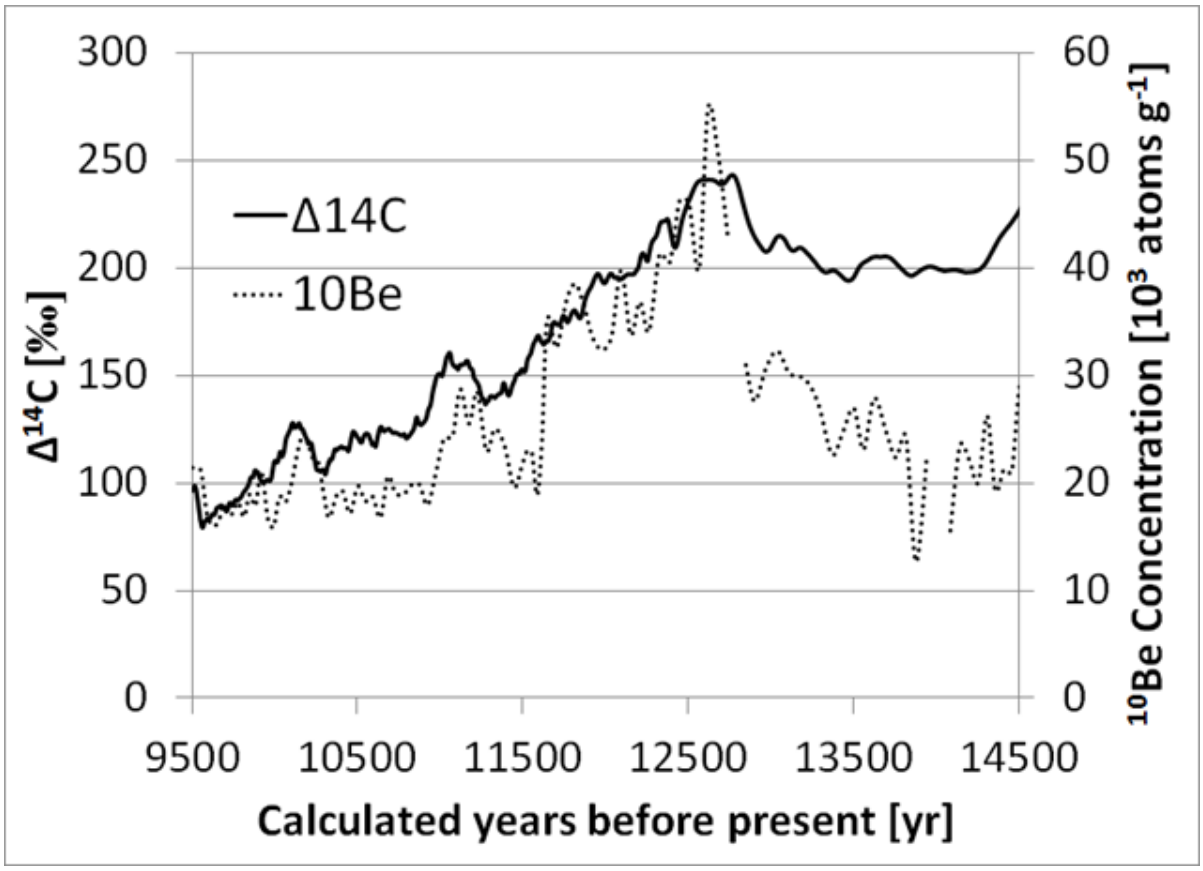

Figure 9: $\Delta^{14}C$ and ^{10}Be concentration measured from 9500 to 14500 years before present. The $\Delta^{14}C$ is measured per mil from tree rings and ice cores and is shown with a solid line, from Stuiver et al. 1998. The ^{10}Be concentration in thousands of atoms per gram of ice is measured from GISP ice cores and is shown with a dotted line, from Finkel & Nishiizumi 1997. This figure displays the sudden increase in both $\Delta^{14}C$ (~5%) and ^{10}Be concentration (~80%) close to the beginning of the Younger Dryas event, at 12900 years before present.

Another offset in carbon dating is seen at 774 AD (Miyake et al. 2012), and this sudden increase of ^{14}C is equal to 1.2% of the total ^{14}C on Earth, which would require a comet roughly 100,000 times more massive than Tunguska. A comet of this size would have caused significant damage near the airburst location and is unlikely because it could have escaped detection only if it occurred far from inhabited areas. Alternately, it has been suggested (Melott & Thomas 2012, Usoskin & Kovaltsov 2012) that this ^{14}C increase may have been caused by a solar major proton event.

Although our results show that ^{14}C can be deposited by extraterrestrial impact, an increase in ^{14}C alone is not conclusive evidence of a past impact. This is due to the other processes which are capable of increasing ^{14}C, such as geomagnetic reversals and variations in cosmic ray flux. This result does, however, suggest that the ^{14}C peak at the Younger Dryas onset does not necessitate an additional process aside from bolide impact.

Our results also show that measurable amounts of ^{10}Be will be deposited in our atmosphere by long-period comets. Although the amount of ^{10}Be could be quite large, measurement of this deposition could be difficult. ^{10}Be is most often recorded through ice core sampling, and the process controlling transport and deposition of atmospheric ^{10}Be to ice sheets is not fully understood (Pedro et al. 2011). ^{10}Be precipitates out of our atmosphere at varying rates depending on geographic location, climate, and other factors. Additionally, ^{10}Be resides in our atmosphere for less than one year on average (Finkel & Nishiizumi 1997), making detection of an instantaneous event very difficult. For these reasons, we find that a lack of ^{10}Be signature typically does not rule out a long-period comet impact. For the proposed Younger Dryas comet, the ^{14}C increase is coeval with a

^{10}Be peak in ice core data, as shown in Figure 9 (Stuiver et al. 1998, Finkel & Nishiizumi 1997). This ^{10}Be peak exists both within the ice core concentration measurements as well as in estimated flux calculations (Finkel & Nishiizumi 1997). An additional effect of the residence time of ^{10}Be being less than the time required for cross equatorial atmospheric circulation (Finkel & Nishiizumi 1997, Melott & Thomas 2009) is that if the conjectured YD impact were predominantly a northern hemisphere event, then a peak in northern hemisphere ice cores coincident without a peak in southern hemisphere ice cores is expected. Our results show that a long-period comet of the size and impact area hypothesized for the Younger Dryas event would contain enough ^{10}Be to create this peak, and would deposit ^{10}Be primarily in the northern hemisphere. Solar proton events or geomagnetic weakening would not show a strong hemispheric asymmetry.

^{26}Al should also be present in comets or asteroids. The deposition process for ^{26}Al is believed to be very similar to that of ^{10}Be. Recent work has focused on the measurement of the ^{26}Al/^{10}Be ratio in ice cores (Auer et al. 2009), and this work found the ratio to remain largely constant through time, but with unexplained increases in older samples of a factor of ~2. The mean ratio of atmospheric ^{26}Al/^{10}Be is 1.89×10^{-3}(Auer et al. 2009). Our results predict the cometary ratio of ^{26}Al/^{10}Be to be ~0.6, and other extraterrestrial objects have been measured to have a ratio of 1 or greater. Cosmic spherules from moraines and deep sea sediments have been measured and show increases in the ^{26}Al/^{10}Be ratio, up to a ratio of 23 (Nishiizumi et al. 1995). This enhancement over the atmospheric ratio occurs due to the location of silicon target nuclei on or near the exterior of extraterrestrial objects. Most silicon on Earth is protected by the atmosphere,

causing ^{26}Al production to be much less than in extraterrestrial objects. All comets and asteroids will have an increased ^{26}Al/^{10}Be ratio for this reason, regardless of orbital period. Therefore, any comet or asteroid impacting the Earth should increase this ratio, as seen in older ice core samples. Because geomagnetic reversals and increases in cosmic ray flux affect all nuclide production uniformly, neither of these phenomena would create this signature. This ratio has been measured in selected sections of the GISP2 ice core (Nishiizumi et al. 2005), but no measurements have been made around the time of the Younger Dryas event. Under current conditions, ~5% of the total ^{26}Al deposited in ice cores comes from extraterrestrial mass (Auer et al. 2009). An impactor of the size hypothesized for the Younger Dryas event would be ~10^4-10^6 times more massive than the yearly average extraterrestrial mass flux, and therefore, would inject many times the average yearly ^{26}Al mass, and deposition of this large amount of ^{26}Al would change the ratio of ^{26}Al/^{10}Be at that time. Assuming the peak in ^{10}Be from GISP ice cores at the Younger Dryas event is from deposition of extraterrestrial matter, the ratio of ^{26}Al/^{10}Be should increase by a factor of ~100+ at that time. The ^{26}Al/^{10}Be ratio is ~1 for all extraterrestrial matter (Auer et al. 2009), and therefore would increase even if the Younger Dryas impactor was not a long-period comet. As ^{10}Be is strongly deposition dependent, and ^{14}C increases can be associated with a variety of phenomena, this ratio proves to be a much better test of the presence of extraterrestrial cosmogenic nuclides within our atmosphere. This ratio should be measured with sufficient resolution for ^{26}Al detection as a test for the Younger Dryas impact hypothesis and would be applicable regardless of impactor type.

We have found that the amount of ^{10}Be and ^{14}C produced in airbursts or impacting long-period comets should be detectable in the geologic record, which can be used to rule out a class of large events. Of known and conjectured cometary airbursts, the Younger Dryas comet remains the only impactor of requisite size for measurable ^{10}Be and ^{14}C deposition. We find that the increases in ^{14}C and ^{10}Be at the time of the Younger Dryas are consistent with the airburst of a long-period comet of the suggested mass, making this a plausible scenario. This is not a conclusive test of whether the event occurred, but rather demonstrates the consistency of the hypothetical Younger Dryas object producing this effect. To properly test the Younger Dryas impact hypothesis, ^{26}Al/^{10}Be ratios must be measured around the time of the purported event. A short lived increase in this ratio would be compelling evidence of a large impact at this time by an extraterrestrial object. Lack of a short lived increase of this ratio from a complete sampling would be inconsistent with a large extraterrestrial impact. We note that due to the expected large increase in ^{26}Al abundance for a large meteor, the required mass of the ice sample is much lower than normally used to examine usual terrestrial ratios. We estimate that the mass of ice required for this measurement would be 5 to10 kg, as opposed to ~100 kg. Future work will measure this ratio across the Younger Dryas boundary as a test of the Younger Dryas impact hypothesis.

5. Conclusion

The numerous effects of cosmic rays comprise a large area of current research. Some researchers have suggested that one such effect is that of climate change, produced by our location within the galaxy. Our work finds no such correlation between spiral arm crossings and the Earth's climate. Despite these findings there are additional effects of cosmic rays, such as secondary radiation by muons and neutrons, which pose a threat to terrestrial biota. Cosmogenic muons are the primary contributors of cosmic radiation to the radiation background. In the case of a nearby supernova or other HECR increasing event, this contribution is increased to the point of becoming a great risk to life. Additionally, at high altitudes cosmogenic neutrons pose a large threat to life. This risk can be greatly increased by SPEs and other cosmic ray increasing phenomena.

Our work developed lookup tables for cosmogenic neutron flux independent of primary spectrum. Unlike previous work, these tables may be used to estimate cosmogenic neutron flux from any cosmic ray increasing phenomenon. As many astronomical events, such as nearby supernovae, have not been measured directly, these tables provide a useful tool for their study. Cosmogenic neutrons produce nuclides, which provide valuable information on past cosmic ray climate when measured in the geologic record. This information is useful for determining the frequency, magnitude, and spectral shape of past events.

In addition to this information, our work shows that cosmogenic nuclide records may be used as a proxy for bolide impacts. Comets and meteors leave residual traces of

cosmogenic nuclides which were contained within their matter when impacting the Earth. We show that measurable increases in ^{14}C and ^{10}Be are expected from large long-period comets but not significant from short-period bolides. Our work provided results of simulations determining the mass of cosmogenic nuclides on long period comets. These results are consistent with the Younger Dryas impact hypothesis and also provide an additional test for the hypothesis. Our results predict the presence of an increased $^{26}Al/^{10}Be$ ratio in ice cores coincident with the Younger Dryas event. A lack of measurable increases in this ratio at that time would be inconsistent with a large bolide impact. In this way we provide a suitable test for the controversial Younger Dryas impact hypothesis. Additionally, this same test could be used as a proxy for other past impact events. As this test does not require the creation of a crater, this test is well suited for airburst comets and other airburst bolides. By locating past impact events within the geologic record, we are better able to determine the rate at which the Earth experiences these biologically threatening phenomena.

6. References

Abassi, R., et al. 2011, Phys. Rev. Letters, 106, 141101

Abassi, R. 2012, Nature, 484, 351–354, doi:10.1038/nature11068

Alberts, W. G., et al. 2001, J. of the ICRU 1, 3

Ackermann, M., et al. 2013, Science 339, 807

Alvarez, L.W., Alvarez, W., Asaro, F., & Michel, H. V. 1980, Science 208, 1095–1108

Aspholm, R., et al. 1999, J.Occup. & Env. Med., 41, 6, 486-491

Atri, D., & Melott, A. L. 2011a. Rad. Physics & Chem., 80, 6, 701

Atri, D., & Melott, A. L. 2011b. Geophys. Res. Let., 38, L19203, doi: 10.1029/2011GL049027

Auer, M., et al. 2009, Earth and Planetary Science Letters, 287, 453

Beck, P. 2009, Rad. Prot. Dos. 136, 244-250

Bissantz, N., Englmaier, P., & Gerhard, O., 2003. MNRAS, 340, 949

Bland, P. A., et al. 1998. Geological Society, London, Special Publications 140, 43-58

Britt, D. T., Consol-magno, G. J., & Merline, W. J. 2006, Lunar and Planetary Science XXXVII

Brown, F.B., et al. 2002, MCNP Version 5, LA-UR-02-3199

Bunch, T. E., et al. 2012, PNAS, 109, E1908-1912

Davis, W. O. 1950, Phys. Rev., 80, 150-154

Dehnen, W., & Binney, J. 1998, MNRAS 294, 429

Delsemme, A. H. 1982, Chemical composition of cometary nuclei (University of Arizona Press, Tucson, AZ)

Dermer, C., & Holmes, J. 2005, ApJ, 628, L21-L24

Dermer, C. 2010, in AIP Conference Proceedings 1279, 191-199

Dias, W. S., & Lépine, J. R. D. 2005, ApJ, 629, 825

Duldig, M. L., et al. 1994, The Ground-Level Enhancements of 1989 September 29 and October 22

Ejzak, L., et al. 2007, ApJ, 654, 373

Englmaier, P., Pohl, M., & Bissantz, N. 2008, Tumbling, Twisting, and Winding Galaxies: Pattern Speeds along the Hubble Sequence, ed. E. M. Corsini & V. P. Debattista (eds.), Memorie della Societa Astronomica Italiana

Erlykin, A. D., & Wolfendale, A. W. 2001, J. Phys. G: Nucl. Part. Phys., 27, 941

Erlykin, A.D., Gyalai, G., Kudela, K., Sloan, T., & Wolfendale, A. W. 2009, JASTP, 71, 1794

Erlykin, A. D., & Wolfendale, A. W. 2010, Surveys in Geophys., 31, 4, 383-398, doi: 10.1007/s10712-010-9097-8

Farinella, P., Foschini, L., Froschle, Ch., Gonczi, R., Jopek, T. J., Longo, G., & Michel, P. 2001, A&A, 377, 1081-1097

Fields, B., et al. 1973, in Proceedings of the Fourth Lunar Science Conference, 2, 2123-2130

Fields, B., Athanassiadou, T., & Johnson, S. R. 2008, ApJ, 678, 549

Finkel, R. C., & Nishiizumi, K. 1997, JGR, 102, 26699-26706

Firestone, R. B., et al. 2007, PNAS, 104, 16016-16021, doi:10.1073/pnas.0706977104

Gehrels, N., et al. 2003, ApJ, 585, 1169-1176

Gies, D. R., & Helsel, J. W. 2005, ApJ, 626, 844

Gillman, M., & Erenler, H. 2008, IJAB, 7, 17

Godwin, H., 1962, Nature, 195, 984

Goel, P.S., 1969, Nature, 223, 1263-1264

Goldhagen, P., Clem, J. M., & Wilson, J. W. 2004, Rad. Prot. Dos., 110, 1-4, 387-392. doi: 10.1093/rpd/nch216

Gomez, G.C. 2006, AJ, 132, 2376

Goncharov, G.N., & Orlov, V. V. 2003, Astron. Rep., 47, 925

Gopalswamy, H., Xie, H., Yashiro, S., & Usoskin, I. 2005, in 29th International cosmic Ray Conference (Pune, India), 1, 169-172

Gordon, M. S., et al. 2004, Nuclear Science, 51, 6, 3527-3434

Grigoriev, A. V., et al. 2010, JGR, 115, A00E52-6, doi:10.1029/2009JA014870

Hagmann, C., Lange, D., & Wright, D. 2007, Lawrence Livermore National Laboratory, Livermore, CA, Tech. Rep. UCRL-TM-229452

Hammer, G. P., et al. 2009, Radiat Protection Dosimetry 136, 232-239

Hayakawa, S., Nishimura, S., & Takayanagi, K. 1961, Publications of the Astronomical Society of Japan, 13, 184

Heck, D. 1999, in DESY Zeuthen (Germany, 1998), Report DESY-PROC-1999-01, 228

Herbst, E., & Cuppen, H. W. 2006, PNAS, 103, 12257

Hess, W. N., Patterson, H. W., & Wallace, R. 1959, Phys. Rev., 2, 116

Hua, Q., et al. 2009, Quarternary Science Reviews, 28, 2982-2990

Hughen, K., Southon, J., Lehman, S., Bertrand, C., & Turnbull, J. 2006, Quaternary Science Reviews, 25, 3216

Indriolo, N., Fields, B. D., & McCall, B. J. 2009, ApJ, 694, 257

Iro, N., Gautier, D., Hersant, F., Bockelee-Morvan, D., & Lunine, J. I. 2003, Icarus, 161, 511-532

Israde-Alcantara, I., et al. 2012, PNAS, doi: 10.1073/pnas.1110614109

Jessberger, E. K., Christoforidis, A., & Kissel, J. 1988, Nature, 322, 691-695

Jetsu, L. 2011, Baltic Astronomy, 20, 289-296

Juckett, D.A., & Rosenberg, B. 1997, Int. J. Biometerol., 40, 206-221

Juckett, D.A. 2007, International Journal of Astrobiology, 6, 307-319

Juckett, D.A. 2009, Int. J. Biometerol., 53, 487-499

Karam, A. 2001, Changes in Background Cosmic Radiation Dose During the History of Life on Earth, Ohio State University dissertation

Karam, A. 2002a, Radiation Physics and Chemistry, 64, 77–87

Karam, A. 2002b, Health Physics, 82, 4, 491-499

Kerr, R. A., 2008, Science, 319, 1331-1332, doi:10.1126/science.319.5868.1331

Kneller, J. P., Phillips, J. R., & Walker, T. P. 2003, ApJ, 589, 217

Kojo, K, et al. 2005, Occupational Environmental Medicine 62, 488-493

Korsun, P. P., Ivanova, O. V., & Afanasiev, V. L. 2008, Icarus, 198, 465-471

Kovaltsov, G. A., & Usoskin, I. G. 2010, Earth and Planetary Science Letters, 291, 182-188

Krankowsky, D., 1991, Comets in the Post-Halley Era, ed. R. L. Newburn, M. Neugebauer, & J. Rahe (Kluwer, Dordrecht) 855

Kurbatov, A.V., et al. 2010, Journal of Glaciology, 56, 747-757

Kusenko, A. 2010, in AIP Conference Proceedings (10/16/2010), 1279, 1, 242

Lal, D. 1991, Earth and Planetary Science Letters, 104, 2-4, 424-439

Lange, H.-J., et al. 1995, Applied Radiation Isotopes, 46, 93-112

Lecompte, M.A., et al. 2012, PNAS, 109, E2960

Levine, E. S., Blitz, L., & Heiles, C. 2006, ApJ, 643, 881

Marochnik, L. S., Mishurov, Yu. N., & Suchkov, A. A. 1972, Ap&SS, 19, 285

Masarik, J., & Beer, J. 1999, JGR, D104, 10, 12099-13012

Masarik, J., & Reedy, R. C., 1995, Earth and Planetary Science Letters, 136, 3-4, 381-395

Medvedev, M. & Melott, A. L. 2007, Astrophysics J., 664, 879-889

Melott, A. L. 2008, PLoS ONE, 3, 12, e4044. doi:10.1371/journal.pone.0004044

Melott, A. L., et al. 2004, International Journal of Astrobiology, 3, 55

Melott, A. L., et al. 2005. GRL, 32, L14808, doi:10.1029/2005GL023073

Melott, A. L., et al. 2008, JGR, 113, E10007, doi:10.1029/2008JE003206

Melott, A. L, & Bambach, R. K. 2011, Paleobiology, 37, 92-112

Melott, A. L., Bambach, R. K., Petersen, K. D., & McArthur, J. M. 2012, J. Geology, 120, 217-226

Melott, A. L., & Thomas, B. 2009, Paleobiology, 35, 311-320

Melott, A. L., & Thomas, B. 2011, Astrobiology, 11, 343-361, doi:10.1089/ast.2010.0603.

Melott, A. L., & Thomas, B. 2012, Nature, 491, E1, DOI 10.1038/nature11695

Melott, A.L., Thomas, B.C., Dreschhoff, G., & Johnson, C.K. 2010, Geology, 38, 355-358

Michel, R., et al. 1997, Nuclear Instruments and Methods in Physics Research B, 129, 153-193

Minchev, I., & Quillen, A.C. 2008, MNRAS, 386, 1579

Miyake, F., Nagaya, K., Masuda, K., & Nakamura, T. 2012, Nature, 486, 240

Mori, M. 1997, ApJ, 478, 225

Moser, M. R., Ryan,, J. M., Desorgher, L., & Fluckiger, E. O. 2005, in Proceedings of the 29th International Cosmic Ray Conference (Pune, India) 2, 421-424

Muscheler, R., et al. 2000, Nature, 408, 567-570

Nakanishi, H., & Sofue, Y. 2006, PASJ, 58, 847

Napier, B., Asher, D. 2009, Astronomy & Geophysics, 50, 1, 1.18-1.26

Nath, B. B., & Biermann, P. L. 1994, MNRAS, 267, 447

Nishiizumi, K., et al. 1995, Meteoritics, 30, 728

Nishiizumi, K., Finkel, R. C., & Welten, K. C. 2005, in Proceedings, The 10th International Conference on Accelerator Mass Spectrometry (September 5-10, 2005, Berkeley, California)

O'Brien, K., et al. 1996, Environment International, 22, 1, S9-S44

Overholt, A. C., Melott, A. L., & Pohl, M. K. 2009, ApJ, 705, L101

Owen, T. 2003, Highlights of Astronomy, 13

Pedro, J. B., et al. 2011, JGR, 116, D23120, 14

Pelowitz, D. B., ed. (2005) MCNPXTM User's Manual. LA-CP-05-0369

Pierce J. R., & Adams, P. J. 2009, GRL, 36, L09820, doi:10.1029/2009GL037946

Plainaki, C., Belov, A., Eroshenko, E., Mavromichalaki, H., & Yank, V. 2007, JGR, 122, A04102-12

Pohl, M., Englmaier, P., & Bissantz, N. 2008, ApJ, 677, 283

Ptuskin, V. 2005, in AIP Conference Proceedings, 745, 1, 14-22

Pukkala, E, et al. 1995, BMJ, 311, 649-652

Rahmstorf, S., et al. 2004, EoS, 85, 48

Ramsey, C. B., et al. 2012, Science, 338, 370

Raup, D.M., & Sepkoski, J.J., Jr, 1984, PNAS, 81, 801

Raymond, J. 2009, Science, 325, 5941, 683-684

Reitz, G. 1993, Radiation Protection Dosimetry, 48, 5-20

Rocha-Pinto, H. J., Scalo, J., Maciel, W. J., & Flynn, C. 2000, A&A, 358, 869

Ruderman, M. 1974, Science, 184, 4141, 1079-1081

Russeil, D. 2003, A&A, 397, 133

Russeil, D., Adami, C., & Georgelin, Y.M. 2007, A&A, 470, 161

Scalo, J., & Wheeler, C., 2002, ApJ, 566, 2, 723-737

Sharma, M., Chen, C., Jackson, B. P., & Abouchami, W. 2009, in American Geophysical Union, Fall Meeting 2009, abstract #PP33B-06.

Shaviv, N. 2003, NewA, 8, 1, 39

Shaviv, N., & Veizer, J. 2003, GSA Today, 13, 4

Smida, R. 2009, in Collision, Proceedings of the International Symposium (Kobe, Japan)

Spitzer, L., Jr., & Tomasko, M. G. 1968, ApJ, 152, 971

Stone, E.C., et al. 1977, Space Science Review, 21, 355

Stuiver, M., et al. 1998, Radiocarbon, 40, 1041

Surovell, T.A., et al. 2009, PNAS, 106, 18155-18158, doi:10.1073/pnas.0907857106

Svensmark, H. 2006, Astron. Nachr., 327, 9, 866, doi:10.1002/asna.200610650

Svensmark, H., Bondo, T., & Svensmark, J. 2009, Geophys. Res. Lett., 36, L15101, doi:10.1029/2009GL038429

The U.S Standard Atmosphere, 1976, U.S. Government Printing Office

Thomas, B., et al. 2005, ApJ, 622, L153

Thomas, B. et al. 2005, ApJ, 634, 509.

Thomas, B., & Melott, A. 2006, New Journal of Physics, 8, 120, doi:10.1088/1367-2630/8/7/120

Thomas, B. et al. 2008, Astrobiology, 8, 1, 9-16, doi:10.1089/ast.2007.0181

Toon, O.B., Zahnle, K., Morrison, D., Turco, R. P., & Covey, C. 1997, Reviews of Geophysics, 35, 41-78

Usoskin, I. et al. 2006, GRL, 33, L08107

Valle, G., Ferrini, F., Galli, D., & Shore, S. N. 2002, ApJ, 566, 252

Vallée, J.P. 2008, AJ, 135, 1301

Vanio et al. 2009, Space Science Review, 147, 187-231

Vink, J. 2009, in AIP Conference Proceedings, 1126, 1, 251-258.

Wainscoat, R.J., Cohen, M., Volk, K., Walker, H.J., & Schwartz, D.E. 1992, ApJ, 400, 516

Wasson, J.T. 2003, Astrobiology, 3, 163–179, doi: 10.1089/153110703321632499

Wissmann et al. 2005, Radiation Measurements, 39, 1, 95-104

Wyckoff, S., Tegler, S.C., & Engel, L. 1991, ApJ, 367, 641

Ziegler, J. F. 1996, IBM J. Res. Development, 40, 1